Optoelectronic Humidity and Temperature Sensor using Apodized Pi-Phase Shifted Fiber Bragg Grating

Navjot Kaur

A Thesis

in

The Department

of

Electrical and Computer Engineering

Presented in Partial Fulfillment of the Requirement

for the Degree of Master of Applied Science at

Concordia University

Montréal, Québec, Canada

January 2019

CONCORDIA UNIVERSITY

SCHOOL OF GRADUATE STUDIES

CONCORDIA UNIVERSITY

SCHOOL OF GRADUATE STUDIES

This is to certify that the thesis prepared

By: **Navjot Kaur**

Entitled: **Optoelectronic Humidity and Temperature Sensor using Apodized Pi-Phase Shifted Fiber Bragg Grating**

and submitted in partial fulfillment of the requirements for the degree of

Master of Applied Science

Complies with the regulations of this university and meets the accepted standards with respect to originality and quality.

Signed by the final examining committee:

_____ Chair

Dr. Ion Stiharu, MIE

_____ Examiner, External

Dr. Ion Stiharu, MIE

_____ Examiner

Dr. Irina Stateikina

_____ Supervisor

Drs. M. Kahrizi & B. Zhang

Approved by: _____

Dr. William E. Lynch, Chair
Gina Cody School of Engineering and Computer Science

_____20_____

_____

Amir Asif, Dean
Gina Cody School of Engineering and Computer Science

Abstract

Optoelectronic Humidity and Temperature Sensor using Apodized Pi-Phase Shifted Fiber Bragg Grating

Navjot Kaur

Humidity control and moisture detection have a wide range of applications in major industries like food storage, chemical plants, electronic instruments, building/construction, medicine, museums and libraries. The most reliable humidity detection methods using capacitors and resistors fail under hazardous operational environments like transformers. Optical gratings based sensors are hence preferred in such conditions due to their properties of light weight, remote sensing and immunity to electro-magnetic interferences.

In this work, an optical humidity sensor based on a rarely investigated FBG is developed. It is called a π-phase shifted fiber Bragg grating (PSFBG). A sharp spectrum signal of PSFBG promises higher resolution in sensing applications. The surface area of the grating developed along an optical cable is coated by a hygroscopic polymer, Polyimide, that undergoes a reversible volume expansion on exposure to humidity. This leads to stress onto the grating and further a shift in the Bragg wavelength.

In order to investigate the electromagnetic wave propagation inside the core of fiber, a study is conducted in COMSOL multiphysics. The implementation of an optical fiber as humidity sensor is modeled. The mechanism of humidity absorption by the polymer layer is simulated and analyzed. Spectral improvements in the sensor signal in terms of interference are implemented using an optimized apodization function. The spectral signal of sensing element is simulated by transfer matrix solution of coupled mode theory in MATLAB. The results of modeling are used to fabricate a sensor containing two 24-mm PSFBGs separated by 12 mm. A distributed feedback laser scanner is used to precisely characterize and evaluate the device performance. The sensor response to changes in humidity and temperature of the environment is recorded. The experimental results are relatively in good agreement with those obtained theoretically.

ACKNOWLEDGEMENT

The completion of this thesis could not have been possible without the direct and indirect support of so many people whose names may not all be enumerated here. Their contributions are sincerely acknowledged and deeply appreciated. However I would like to extend my special thanks and indebtedness to

Dr. Mojtaba Kahrizi of Electrical and Computer Engineering Department and Dr. Bowie Zhang, for investing their time & energy in guiding me through the entire project.

Personnel of Electrical and Computer Engineering at Concordia University and the Natural Sciences and Engineering Research Council (NSERC) for their financial support.

Parsoua Abedini and Sevin Samadi, for their help in COMSOL simulations and countless discussions in shaping the path of this project.

Mr. Peter Kung and Mr. Chaska Durand from QPS Photronics Inc. for facilitating various equipments to perform the experiments reported in this work and for their help in LabVIEW.

The Anonymous referees for their useful suggestion throughout the publication of this research.

My darling brother Harjot for constantly listening, supporting and understanding.

Above all, the great almighty, the author of knowledge and wisdom, for his countless blessings.

I dedicate this work to my dear mother and father whose love, courage and devotion has been the strength of my striving.

Navjot K Sidhu

.

List of publications and conference contributions

1. N. K. Sidhu, P. A. Sohi, and M. Kahrizi, “Polymer based Optical Humidity and Temperature Sensor,” J. Mater. Sci. Mater. Electron, 2019.
2. N. K. Sidhu, P. A. Sohi, S. Samadi, and M. Kahrizi, “Modeling of FBG Moisture sensor in COMSOL,” Photonics North, 2018, p. 1.
3. N. K. Sidhu, P. Kung, and M. Kahrizi, “Apodized Pi-PSFBG Moisture / Temperature Sensor,” Photonics North (PN), 2018, p. 1.
4. N. K. Sidhu, P. A. Sohi, and M. Kahrizi, “Modeling Time dependent Humidity Diffusion into FBG Polyimide Coating for Sensing Applications,”2018, ICOOPMA.
5. N. K. Sidhu, Bowei Zhang, P. Kung, M. Kahrizi,” Development of apodization profile for highly sensitive pi-phase shifted fiber Bragg grating moisture and temperature sensor”,2018, ICOOPMA.

Table of contents

Table of Figures

List of tables

List of Abbreviations

RH	Relative humidity
SH	Saturation humidity
PPMv	Parts per million by volume
EMI	Electromagnetic interference
RFI	Radio frequency interference
SMF	Single mode fiber
FBG	Fiber Bragg grating
DFB	Distributed feedback
$\boldsymbol{\pi}$ –PSFBG	Pi-phase shifted fiber Bragg grating
pm	Pico meter
TIA	Transimpedance amplifier

1 Introduction

1.1 Humidity basics and the measurement parameters

Humidity is the amount of water vapour in air or other gases. There are diverse ways to state and quantify humidity.

1.1.1 Absolute humidity

Absolute humidity is the ratio of the mass of water vapour in air to the volume of air. It can be expressed as[1]

$$AB = \frac{m_w}{v} \tag{1.1}$$

where m_w is the mass of water vapour in grams or grains (1 grain = $\frac{1}{7000}$ pound lb.), v is the volume of air in m^3 or ft^3 and AB is the absolute humidity in g/m^3 or $grains/\ ft^3$.

1.1.2 Relative humidity

Relative humidity (RH) is defined as ratio of the amount of moisture content of air to the saturated moisture level that the air can hold at a same given temperature and pressure of the gas. It is the most commonly used measure of humidity and is expressed as[1]

$$RH\% = \frac{P_V}{P_S} \times 100 \tag{1.2}$$

where P_V is the actual partial pressure of moisture content in air and P_S the saturated pressure of moist air at the same given temperature (both in Bar or KPa).

RH is a relative measurement because it is a temperature dependent magnitude.

1.1.3 Saturation humidity

Saturation humidity (SH) is the ratio of the mass of water vapour at saturation to the volume of air. It is a function of temperature and can provide the maximum amount of moisture content (mass) in a unit volume of gas at a given temperature.

$$SH = \frac{m_{ws}}{v} \tag{1.3}$$

where m_{ws} is the mass of water vapour in g and v is the volume of air in m^3 [1].

1.1.4 Parts per million by volume (PPMv)

Parts per million by volume (PPMv) is defined as volume of water vapour content per volume of dry gas, and parts per million by weight (PPMw) is obtained by multiplying PPMv by the mole weight of water per mole weight of that gas or air. PPMv and PPMw are among the absolute humidity measurements.

1.1.5 Dew point and frost point

D/F point are functions of the pressure of the gas, but independent of temperature and are amongst the methods of absolute humidity measurements. Dew point is defined as a temperature (above 0 °C) at which the water vapour content of the gas begins to condense into liquid water. Dew point in an air atmosphere is the temperature at which the saturation water vapour pressure is equal to the partial pressure of the water vapour. Frost point is the temperature (below 0 °C) at which the water vapour in a gas condenses into ice. The difference between the ambient temperature and the dew point temperature is a measure of the ambient relative humidity.

Humidity measurement is crucial process wherever there is a need to prevent condensation, corrosion, warping, mould, or other spoilage of products. This is highly relevant for industries like foods, pharmaceuticals, chemicals, fuels, wood, paper, and many others. Various humidity sensing techniques are employed to detect presence of minute water content before the damages happen [2]. Next section discusses the available technologies for humidity detection and evaluates their pros and cons.

1.2 Sensors for the humidity/moisture measurement

Humidity/moisture sensors work by detecting minute changes that alter electrical currents or temperature in the air in order to calculate the presence of humidity. Long before optical sensors, moisture sensors worked based on resistive, capacitive and thermal conductivity measurement methods[3], [4].

1.2.1 Capacitive humidity sensors

Capacitive humidity sensors comprise of a thin film of a hygroscopic dielectric material deposited between the two conductive electrodes fixed onto a substrate[5]. The properties of the sensor are determined by the choice of polymer material and the geometry of electrodes. The sensor responds to the humidity variations by varying their dielectric constant which is directly proportional to the changes in water vapour around it. Figure 1.1 depicts the schematic of a capacitive humidity sensor.

Major drawback to the capacitive humidity sensors is that the distance from the sensor to the signaling circuit is very limited which makes them unsuitable for remote operations.

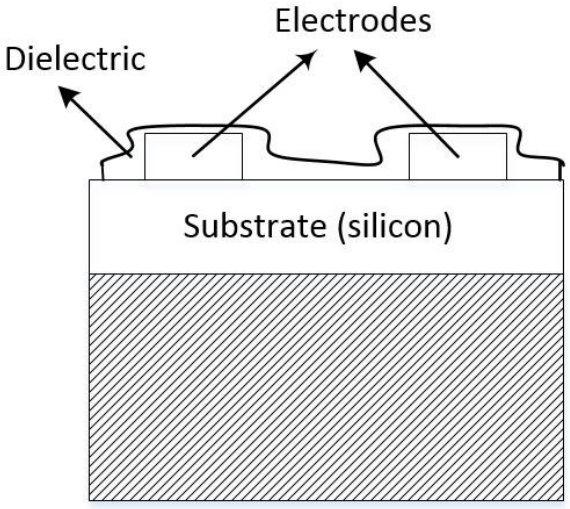

Fig. 1.1 Schematic of a capacitive humidity sensor. Modified from internet.

1.2.2 Resistive humidity sensors

The working principle behind resistive sensors is that the resistivity/conductivity of non-metallic conductors is dependent on the water content inside them. These sensors are fabricated by calcination of low resistivity metals like gold and ruthenium oxide in shape of a comb like pattern. This particular structure is adopted to increase the contact area of the sensor. A polymeric film is deposited on the electrodes which acts as a humidity sensing film. Upon moisture ingress at the

topmost layer, the resistivity between the electrodes change. A simple electric circuit is used to measure the changes in resistivity.

Resistive humidity sensors are small sized, low cost, easy to calibrate devices. They eliminate the drawback of capacitive humidity sensors in terms of remote control operations. However, these devices are sensitive to chemical vapours and contaminants. Hence their application is limited to certain environments only. Figure 1.2 shows the schematic of a resistive humidity sensor.

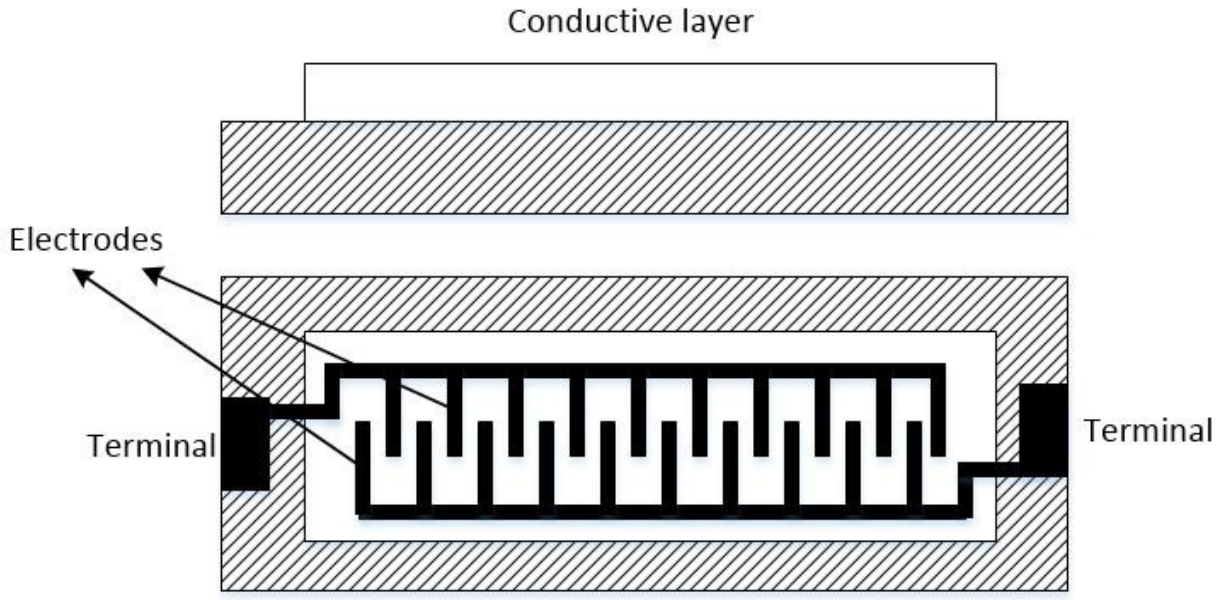

Fig. 1.2 Schematic of a resistive humidity sensor. Modified from internet

1.2.3 Thermal conductivity humidity sensors

Thermal conductivity humidity sensors (also known as absolute humidity (AH) Sensors) measure the thermal conductivity of both dry air as well as the humid air. They work with two thermistors in a circuit, one of which is hermetically sealed in a chamber filled with dry Nitrogen while the other is exposed to open environment through small venting holes. When the circuit is switched on, the difference between the resistances of two thermistors is directly proportional to the absolute humidity around the sensor. The schematic of a thermal conductivity humidity sensor is presented in figure 1.3.

Thermal conductivity sensors provide higher resolutions as compared to the capacitive and resistive types of sensors but the presence of any other gas whose thermal properties are different than the Nitrogen affects the readings of the obtained measurements.

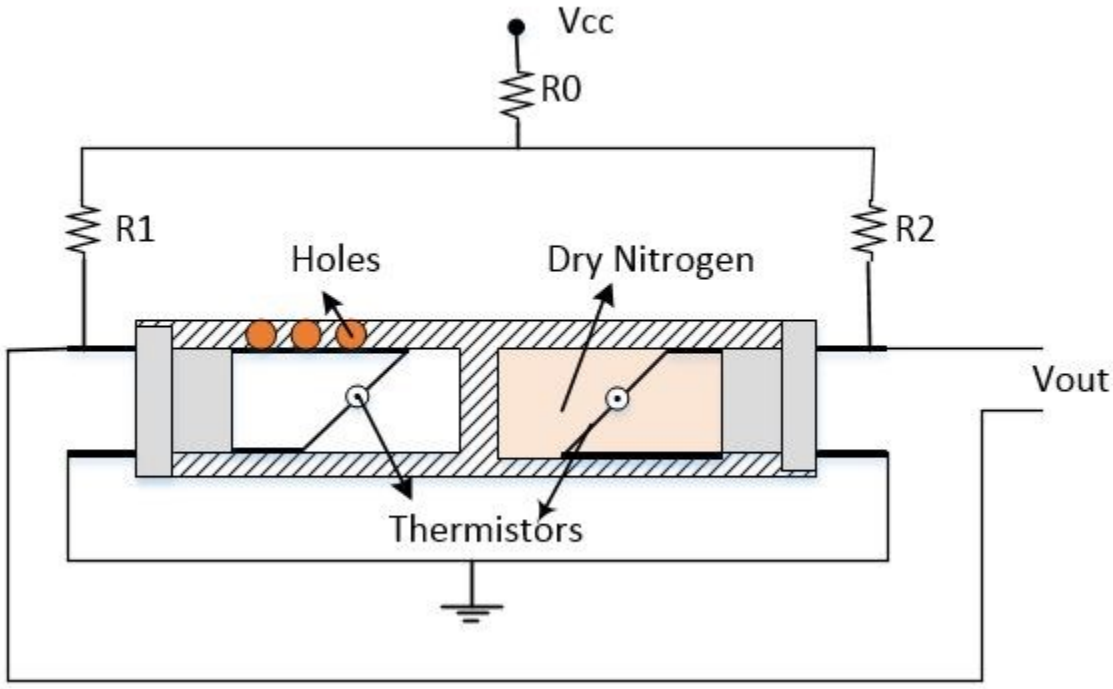

Fig. 1.3 Diagram of a thermal conductivity humidity sensor. Modified from internet

To conclude, the performance of all three types of sensors explained in this section is limited to few environment and applications due to their inability to function in environments involving explosive materials, chemical vapors, and high temperature and voltage conditions. This led the researchers to explore the possibility of moisture/humidity sensing through optical fibers.

1.2.4 Optical sensors

Initially, Optical sensors used the amplitude, polarization, frequency and the phase of a harmonic electromagnetic wave to perceive the information regarding air humidity. An electromagnetic wave can be represented as

$$E(t) = E_0 \cos(\omega t - \varphi) \tag{1.4}$$

where E_0 is the amplitude, ω is the frequency and φ refers to the phase of the wave.

The presence of moisture, temperature or any specific gas can be detected using optical sensors.

In the process of developing the optical sensors towards greater sensitivity, precision, adaptability, compactness and intelligence, fiber optic technology was explored. Optical fibers have numerous properties like small size, light weight, water-resistance, thermal stability, corrosion-resistance and remote monitoring capability. In environments with intolerable heat or radiation levels they can play a significant role in measurement or monitoring. They also show immunity to electromagnetic (EMI) and radio frequency (RFI) interferences. Consequently, modern fiber optic sensors have become replacements to the traditional electromagnetic sensors.

1.3 Historical perspective on the optical fiber Bragg grating humidity sensors

Fiber Bragg grating (FBG) is a periodic modulation of refractive index , photo-induced on a short segment of an optical fiber [6]. First reliable method of its fabrication was devised by Meltz *et. al* in 1989 by producing the grating with reflectivity of 50-55% and full width at half maximum of 42 GHz using a transverse holographic technique [7]. Since then, FBG has been researched for its application as an optical sensing element. Infact, it is the most widely studied technology for optical fiber sensors. Properties of the optical signal (e.g. intensity, phase, polarization, or wavelength) can be modulated in response to the changes in physical parameters (e.g. strain, temperature, and pressure) in the environment surrounding it [8]–[10]. FBG sensors have advantages like small size, high sensitivity, ability to perform under rugged environmental conditions, electrical passiveness, and immunity to electromagnetic interference[11]–[13].

Optical humidity sensing using FBG requires a mechanism to establish an indirect interaction with the properties of optical signal. It is well known that strain can directly modulate the grating period of FBG in response to which Bragg wavelength shifts[14]–[16]. So, fiber containing FBG is coated with a hygroscopic polymer that undergoes reversible volume expansion on exposure to the

humidity [17]. Hence strain is imposed indirectly on the FBG in response to which Bragg wavelength shift is recorded [17], [2].

Polyimide coated uniform FBGs were first explored for relative humidity (RH) sensing by Limberger et al. in [18]. FBG with a polyimide coating of thickness 18.5 µm and a bare FBG were exposed to relative humidity and temperature range of 10 RH% to 90 RH% and 23 °C up to 50 °C, inside a climate chamber. The device shows maximum Bragg wavelength shift of more than 0.5 nm at 1550 nm. Linear function for the relative Bragg wavelength shift vs. relative humidity was reported in this work. Unlike previous experiments with different polymers, the RH influence on the polyimide was found to be quite reversible [18]. Kronenberg et al. further explored a linear array of a bare FBG with seven Pyralin-recoated FBGs of varied coating thicknesses ranging 3.6 to 29.3 mm[19]. Sensor was characterized and calibrated in the climatic chamber with humidity ranging 10–90% RH and temperature ranging 13–60 °C. The proposed sensor design was easy to implement because of its multiplexing capabilities. The experimental results proved that the T and RH sensitivities were determined by the coating thickness, with the sensor becoming more sensitive with increasing coating thickness.

A high RH sensor using gelatin coated long period grating (LPG) was proposed by Tan et al. in 2005[20]. LPG was inscribed by amplitude mask technique inside the hydrogen loaded, corning-SMF-28 optical fiber. The gelatin solution was prepared as ratio 1 g of gelatin to 20 g of distilled water, heated up to 65 °C. Dip coating was used for the coating gelatin onto the fiber. The experiments were conducted in humidity range of 43%- 99% RH at 25 °C. Gelatin was found to be highly sensitive between 90 and 99%RH with sensitivity of 0.833%RH, resolution of ±0.00833%RH and accuracy of ±0.25%RH.

Wang et al. proposed a theoretical analysis of four-layered step index waveguide model to explain the variations of Bragg wavelength of LPG moisture sensor coated with hydrogel [21]. A hydrogel with refractive index higher than the refractive index of cladding was obtained by adjusting the proportions of acrylic acid, vinyl pyridine, benzoyl peroxide and N,N'-dimethyl bisacrylamide. The experimental investigation showed the resonant wavelength shift of 11.3 nm from 38.9% to 100% at 25 ± 2 °C, with an accuracy of ±2.3% RH. Huang et al. proposed a scheme for utilizing thermoplastic polyimide-coated fiber Bragg grating (FBG) to measure the RH in [22]. A 2.5 cm long and 8µm thick thermoplastic polyimide layer was coated onto a standard SMF-28 fiber

containing FBG. The low-cost coarse wavelength division multiplexing (CWDM) was used to interrogate the Bragg wavelength. The experimental results demonstrated that the sensor exhibited a high sensitivity over the response time of approximately 5 s over a wide range of RH (11% – 98%).

A wider functioning range of 4% to 96% RH was demonstrated by a moisture sensor reported by Aneesh et al. in [23]. The sensor was coated with a nanostructured sensing film of zinc oxide doped sol–gel, synthesized over a centrally decladded optical fiber. The device was based on the phenomenon of intensity modulation through evanescent wave absorption. A small portion of the optical power in the cladding region altered the fiber output after interaction with the sensing film. Output of fiber corresponding to the applied RH was highly linear and fast in terms of the response time.

A fully optical sensor with response time and resolution comparable to the current capacitive relative humidity (RH) sensors was presented in [24]. Several gratings of 2 mm length were etched to get the diameters ranging 20 μm -120 μm. The gratings with the reduced fiber diameter were coated with ∼2 μm thick Pyralin. Experiments were conducted to test the sensors under 30% to 90% RH conditions at 24.0 ± 0.2 °C. The data yielded RH sensitivities in the range 0.23 to 1.42 (±0.01 (10^{-6} $\%RH^{-1}$)). The observations exhibited that by decreasing the diameter of fiber, highly sensitive, linear and reversible sensor can be obtained with even the low coating thickness. The transient results showed that the sensors response time was as low as 3.2 sec.

An increased sensitivity and durability for moisture detection was reported using a Bragg grating coated with organo-silica hybrid material in [25]. Post the coating process, the FBG had an average diameter in range 375 ± 5 μm and 591 ± 5 μm. The maximum sensitivity reported was of 22.2 pm/%, saturated in the duration of 16.4 ± 0.4 minutes. A simple, low cost and fast response time polymer optic fiber Bragg grating (POFBG) based humidity sensor was reported by Rajan et al. in [26]. A high quality etched POFBG with a diameter of 25 μm was prepared by acetone-methanol etching method. System sensitivity of 0.23 mV/%RH was achieved experimentally within a response time of 4.5 s. Further observations yielded a non- linear decrease in response time with a decrease in the POFBG diameter.

Three different polyimide coatings, Avensys PI, P84 and P84 HT, were investigated in 2015 by Swanson et al. in [27]. The experiments confirmed that the sensor with 53 μm thick coating of P84

HT polyimide coating yielded the most promising coefficient of moisture expansion, 73.8 ppm/% RH. Experiments on P84 polyimide coatings showed that the sensitivity could be improved by increasing the coating thickness and reducing the fiber diameter. However, this would increase the sensor response time.

A humidity sensing network made from five ultra-weak fiber Bragg gratings (UWFBGs) was proposed by Bai et al. in [28]. All the FBGs were dip-coated with a silane coupling agent before coating them with polyimide ZKPI-305IIE of various thicknesses. Different salt solutions were used to obtain the range of RH concentrations, from 23% to 83 %RH at 28.5°C. The RH sensitivities obtained after experiments were 1.134, 1.633, and 1.639, 1.770 and 1.832 pm/% RH, for 12.7μm, 36.9μm, 39.3μm, 51.8μm, 55.3μm, respectively.

Recently, a photonic based humidity sensor using carboxymethyl cellulose (CMC) coating on the fiber containing FBG was reported by Hartings et al. in [29]. The fiber was dip-coated into an aqueous solution (5% by mass) of CMC. Strain induced in fiber due to the water adsorption properties of CMC was read out as a frequency change in the resonance of the photonic device. The results proved a linear dependence on humidity over the RH range of 5%–40% with the response time of a minute.

1.4 Scope of the thesis

Although various fiber optic sensors exist for moisture and temperature detection, development of new sensing schemes aids understanding and provides improvements for these devices. In this thesis, it is attempted to design, simulate and test a polymer coated optical moisture sensor made from apodized, π- phase shifted fiber Bragg grating (π-PSFBG). π-PSFBG is an advanced grating, recently underlined for their spectral characteristics. Phase shift of π is induced in a uniform grating, which opens a very narrow transmission band in the stop band of grating spectrum [30], [31]. This accounts for a very steep slope in the peak area, hence effectively improving the sensing ability of system[32].

Through finite element modeling and simulations using COMSOL, we comprehensively research the design parameters of polymer coating used in the moisture sensor. Moisture absorption by the polyimide as a function of time is studied. The model includes transport of diluted species physics

to analyze the moisture diffusion into the polyimide-layers. The effect of polyimide thickness on the induced strain and deformed geometry of the fiber is modeled.

For best spectral characteristics, the concept of apodization of π-PSFBG is explored in MATLAB. When multiple gratings are inscribed into a single fiber to implement a series sensing network, side-lobes of the gratings can induce significant interference. This degrades the sensor spectrum and hence sensibility of the device. To improve the side-lobe suppression of grating, the refractive index in the core is modulated with an apodization profile. Here, in this research, an appropriate apodization profile is used to simulate spectrum signal of apodized π-PSFBG. A model of the sensor has been simulated that shows the wavelength shift with respect to the changes in the grating period.

Finally, a moisture sensor is fabricated by inscribing two apodized π-PSFBGs (separated by 12 mm) in a fiber based on parameters obtained from the simulated model. The sensor is then tested under various environmental conditions for its moisture, temperature and response time characteristics. The proposed thesis titled "Optoelectronic Moisture and Temperature Sensor using Apodized Pi-Phase Shifted Fiber Bragg Gratings" consists of seven chapters. The first Chapter of the thesis provides an introduction and a historical review of fiber optic moisture sensors and thesis overview. The summary of the thesis is discussed in the next section.

1.5 Overview of the chapters

Thesis begin with a simple introduction to light propagation inside optical fibers in chapter 2. Details on the geometry of a typical fiber and the laws of optics governing the light wave inside the fiber are discussed. Optical fiber Bragg gratings, their classification and various methods for their fabrication have been reviewed. In the final section, the application of Bragg gratings in the field of humidity sensing is explored. The design, principle and operation of optical fiber Bragg grating humidity sensor have been illustrated.

Chapter 3 is on the finite element analysis of an optical fiber humidity sensor in COMSOL wave optics module. The design of model is reported step by step in three sections. First section explains the model of a simple optical fiber Bragg grating to study the electric field distribution inside it. The reflection and transmission characteristics of the grating are simulated in this section.

Since the fiber is directly insensitive to humidity, second section summarizes the process of making the optical fiber respond to humidity in its surroundings through a material coating. Simulation results showing the changes in the electric field pattern inside the fiber core after the optimum choice of material proves the behavior of optical fiber as humidity sensor. Finally, the effect of humidity on the reflection characteristics of grating is presented in the results.

Section third of this chapter reports the complex 3D model of a fully optical humidity sensor in COMSOL environment. Results of the simulations relate the thickness of the material coated on fiber with the strain it induces after being prone to the humidity and further with the extent of fiber geometry deformed through this strain. The model also simulates the response time characteristics of the sensor with respect to various coating thicknesses.

Chapter 4 begins with the coupled mode theory and the effect of refractive index variations inside the fiber. The scope of modulating the refractive index of the grating with an apodization profile is discussed. A π-PSFBG is explored as a sensing element and MATLAB is used to simulate its spectrum characteristics before and after the apodization. The sensitivity of π-PSFBG with respect to strain and temperature is also simulated in this chapter.

Chapter 5 looks in the fabrication of the polymer coated, apodized $\boldsymbol{\pi}$-PSFBG humidity and temperature sensor as modelled in chapter 3 &4. In order to calibrate the fabricated sensor, a distributed feedback laser scanner setup is built with the help of QPS Photronics inc. details of which are included in this chapter. Finally, the chapter elaborates the user interface used for monitoring the sensor response during calibration, which is designed in the LabVIEW environment.

Chapter 6 presents the design of experimental setups for measuring the sensitivity of sensor with respect to humidity as well as temperature. Detailed experimental analysis of π-PSFBG humidity sensor in the laboratory is reported in this chapter. The sensitivity of the sensor with respect to humidity and temperature is determined. The response time characteristics and reversibility of sensor is tested and compared with the simulation results in chapter 3&4.

Chapter 7 summarizes the conclusion of this thesis and presents some ideas for the future work in this field.

2 Theoretical background

2.1 Aim

This chapter outlines the geometry and the physics of optical fibers. A short review of Snell's law and total internal reflection is done to underline the wave propagation through the fiber. Fiber Bragg gratings and their types are also introduced in this chapter. Interferometric, phase mask and point by point method: three of the many proposed schemes for grating inscription, are reviewed and some salient features of these methods are discussed. Towards the end, we elaborate the working principle of a humidity sensor using optical fiber Bragg gratings.

2.2 Principle of the light propagation in the optical fibers

The optical fibers enabling light transmission through them consist of 3 subcomponents- core, cladding and the jacket. Core of the fiber is the medium through which the light propagates. It is made of silica and may have an overall diameter of 8 μm for single mode or 50 μm or 62.5 μm for multimode transmission. Core is surrounded by a thick layer of cladding that has lower refractive index than that of the core. Regardless of the core construction, the cladding has an overall diameter of 125 μm. A protective coating cushioning material like acrylate is used to add strength and build up the outer diameter to about 250-μm. Plastic Jacket is applied over the buffer jacket to create a tight-buffered optical fiber. Up to 12 tight buffered optical fibers are then encircled to provide greater environmental protection in form of a finished optical fiber cable. Figure 2.1 shows the 3-D geometrical diagram of an optical fiber. Core, cladding and the jacket with subsequent diameters are labeled in the diagram.

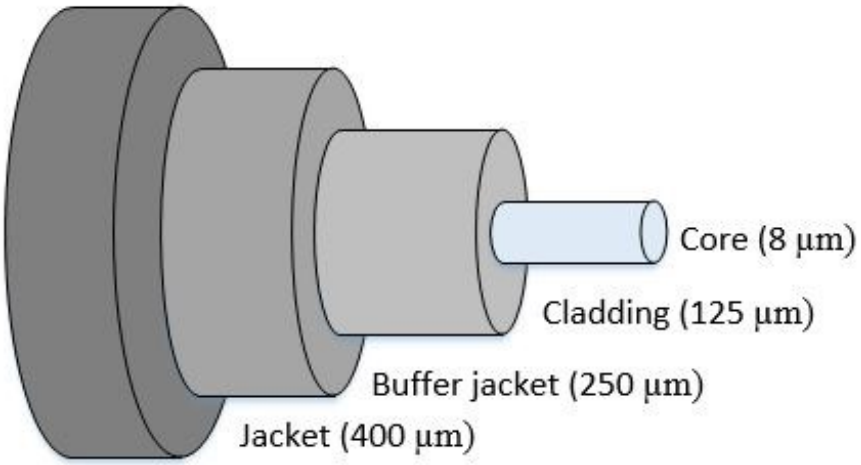

Fig. 2.1 Cross section of an optical fiber. Modified from internet.

The material and geometry of optical fiber makes it behave as a waveguide, i.e. a device that can transmit light (electromagnetic radiation) over long distances with a little dispersion. According to geometrical optics, when a plane wave strikes at a boundary between two media with different refractive indices, the light is partially reflected and partially transmitted into the second medium, according to Snell's law[33],

$$n_1 Sin\theta_i = n_2 Sin\theta_t \tag{2.1}$$

where n_1 is the refractive index of the core, n_2 is the refractive index of the cladding, θ_i is the angle of a light beam heading for a core-cladding boundary and θ_t is the angle of the light beam that leaves the boundary (refer figure 2.2).

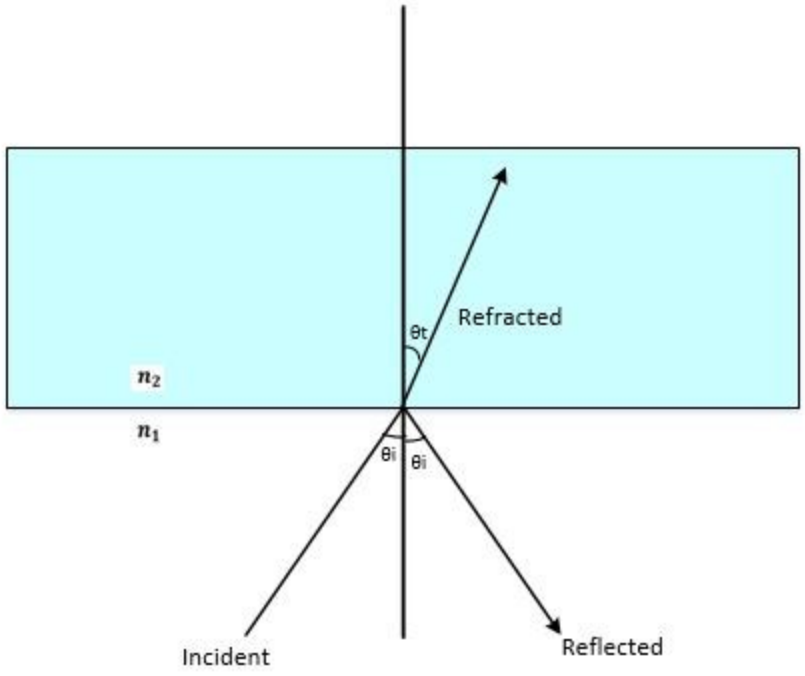

Fig. 2.2 Snell's law of refraction

If $n_1 > n_2$ and the angle θ_i is large enough, the refracted light is zero, i.e. total internal reflection occurs due to which the light does not leave the fiber. It can travel down a fiber-optic cable for 80-100 km by bouncing repeatedly off the core-cladding interface. A single mode optical fiber (SMF) is designed to carry a single light ray over a long distance. The core of this fiber is about 5-10 μm in diameter. Light inside the SMF travels without bouncing off the edges. A multimode fiber, on the other hand, is used for short distance applications. It is about ten times larger in diameter than a single mode fiber. As the name multimode suggests, the light beams can travel through the core by following a variety of different paths, each at a slightly different reflection angle within the optical fiber core.

2.3 Introduction to optical fiber Bragg gratings

In one of the several applications of optical fibers, a small segment inside the core of fiber is made to behave as a distributed Bragg reflector. The refractive index inside the core of this segment is periodically varied by a strong UV. The periodic index variations (known as gratings) are the

planes formed perpendicular to the axis of fiber. When light is guided through the fiber Bragg gratings (FBGs), it is scattered at each plane. In general, the reflected light will get progressively out of phase and will tend to cancel. However, for a narrow set of wavelength, the Bragg resonance condition is satisfied. In that case, light at these wavelengths will be scattered in phase at the successive index planes. Under such phase matching conditions, FBG couples the forward propagating core mode to the backward propagating core mode as shown in figure 2.2. This results in a narrow band of reflected light with a sharp reflectance peak at the center called the Bragg wavelength.

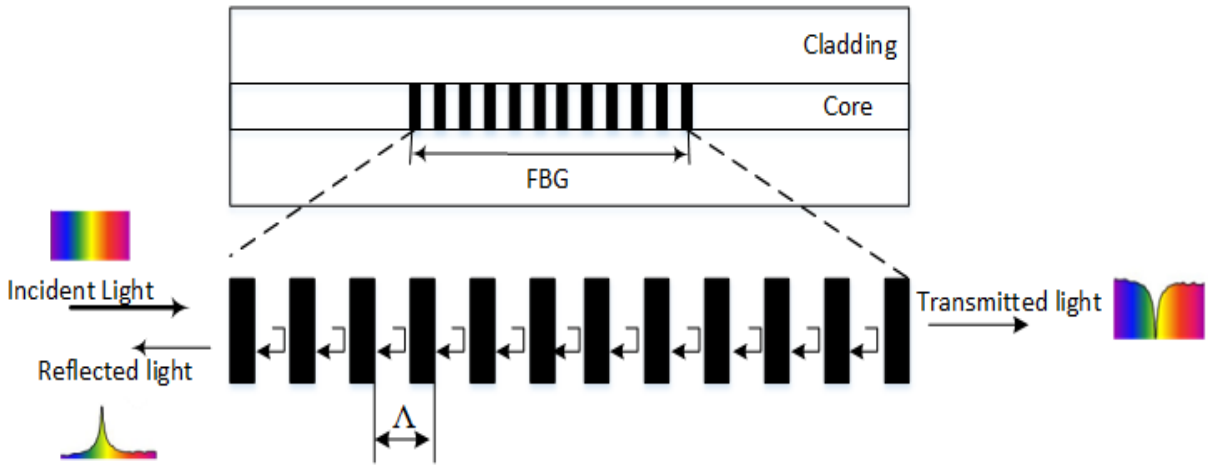

Fig. 2.3 Working of an optical fiber Bragg grating. Modified from[34]

2.3.1 The Bragg resonance condition

The Bragg resonance condition is based on the principle of energy and momentum conservation. Energy conservation requires that the frequency of the incident radiation is equal to the frequency of the reflected radiation. Momentum conservation requires the sum of incident wave vector, K_i and the grating wave vector, K, is equal to the wave vector of the scattered radiation, K_f,

$$K_i + K = K_f \tag{2.2}$$

where the grating wave vector, K, has a magnitude $\frac{2\pi}{\Lambda}$, (Λ being the grating period shown in figure 2.3) and direction normal to the grating planes. The diffracted wave vector is equal in magnitude

but opposite in direction to the incident wave vector. Hence, the momentum conservation condition becomes,

$$2\frac{2\pi n_{eff}}{\lambda_b} = \frac{2\pi}{\Lambda} \tag{2.3}$$

which simplifies to the first-order Bragg condition

$$\lambda_b = 2\, n_{eff}\Lambda \tag{2.4}$$

where the Bragg wavelength, λ_b , is the free-space center wavelength of the input light that will be back reflected from the Bragg grating, and n_{eff} is the effective refractive index of the fiber core at the free-space-center wavelength.

The FBGs are distinguished either by the spacing between the grating planes (grating pitch/period) or the angle between grating planes and fiber axis (tilted FBG). The most common type of grating has a constant period (typically 0.22-0.54 μm) as depicted by figure 2.3. Depending on the length of grating and the magnitude of induced index change, this grating can function as a narrow-band transmission or reflection filter. In combination with other similar gratings, these devices can be arranged to function as bandpass filters. Few other popular Bragg gratings are listed here.

2.3.2 Long period gratings

The grating period in long period grating is typically 100-500 μm. The forward propagating core mode is coupled to one or a few forward propagating cladding modes. Acting as loss filters, these gratings can be used in gain equalization.

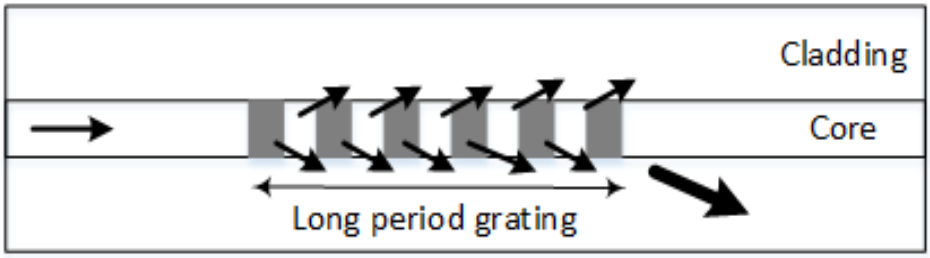

Fig. 2.4 Long period grating

2.3.3 Tilted fiber Bragg gratings

The grating planes in tilted fiber Bragg grating are at a certain angle to the axis of fiber. Such slant planes can couple a forward propagating core mode to backward propagating core mode and backward propagating cladding mode. These loss gratings are used for gain equalization in erbium-doped fiber amplifiers.

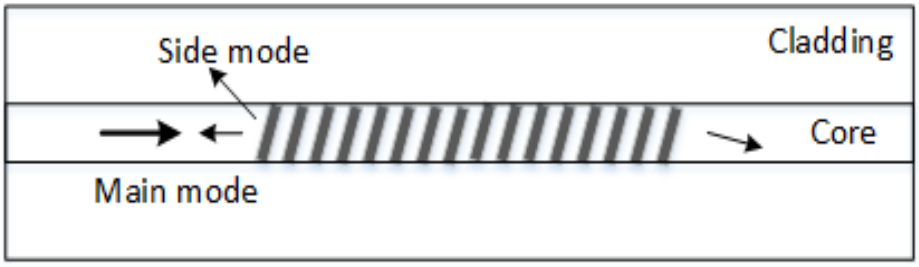

Fig. 2.5 Tilted fiber Bragg gratings

2.3.4 Chirped fiber Bragg gratings

A chirped fiber Bragg grating has a monotonically varying grating period as shown in figure 2.6. Such grating period can be realized by axially varying either the grating period or the index of refraction of the core or both. Resulting reflection spectrum is wider and each wavelength component is reflected at different positions, which results in delay time difference for different reflected wavelengths.

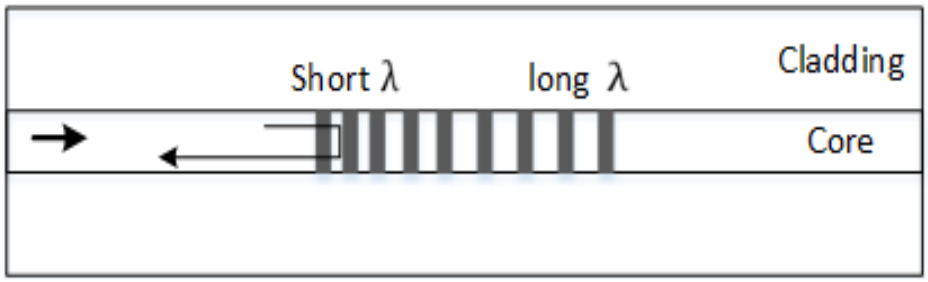

Fig. 2.6 Chirped fiber Bragg gratings

2.3.5 Apodized gratings

In apodized gratings, the profile of the index modulation along the fiber length is given a bell-like functional shape as shown in figure 2.7. The index modulation is weak at both the ends and high

at the center, which decreases the effective length of the grating. Apodization of grating results in sharp spectral response and eliminates the reflectivity of the side lobes.

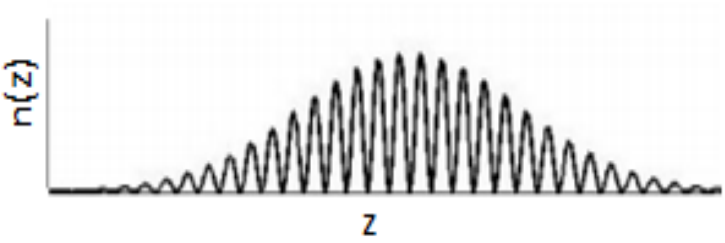

Fig. 2.7 Gaussian apodized refractive index function

2.4 Methods of fabrication of optical fiber Bragg gratings

There are three commonly used methods for writing FBGs

2.4.1 Interferometric method

In the interferometric method a laser beam is spilt into two and directed with mirrors in a way that the two beams intersect create and form an interference pattern on the fiber (figure 2.2). The refractive index on the points of maxima of the interference pattern increases thus creating the fringe pattern or grating. The properties of this fringe pattern can be changed by changing the position and angle of mirrors and other components. However, the use of many mechanical components increase vibrations in the system.

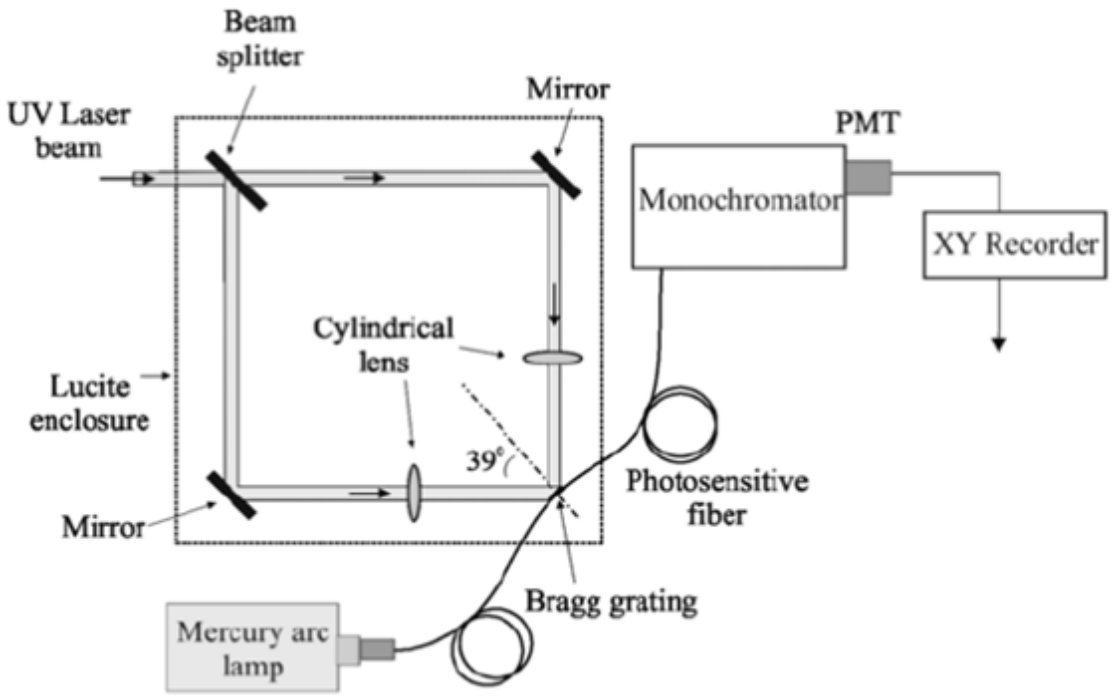

Fig. 2.8 Interferometric method of fiber Bragg grating inscription. Modified from [7]

2.4.2 Phase mask technique

Phase mask technique is one of the most effective methods for writing Bragg gratings in the photosensitive fiber. This method employs a diffractive optical element (phase mask) to spatially modulate the UV beam. A phase mask is a transparent plate with a slit pattern inscribed. The light directed at the phase mask splits up in zero order and higher order which makes it easy to suppress the zero order. The higher order beams are focused on a fiber to create the FBG. The phase mask method does not suffer from the mechanical vibration problems that the interferometric method does and is therefore preferable.

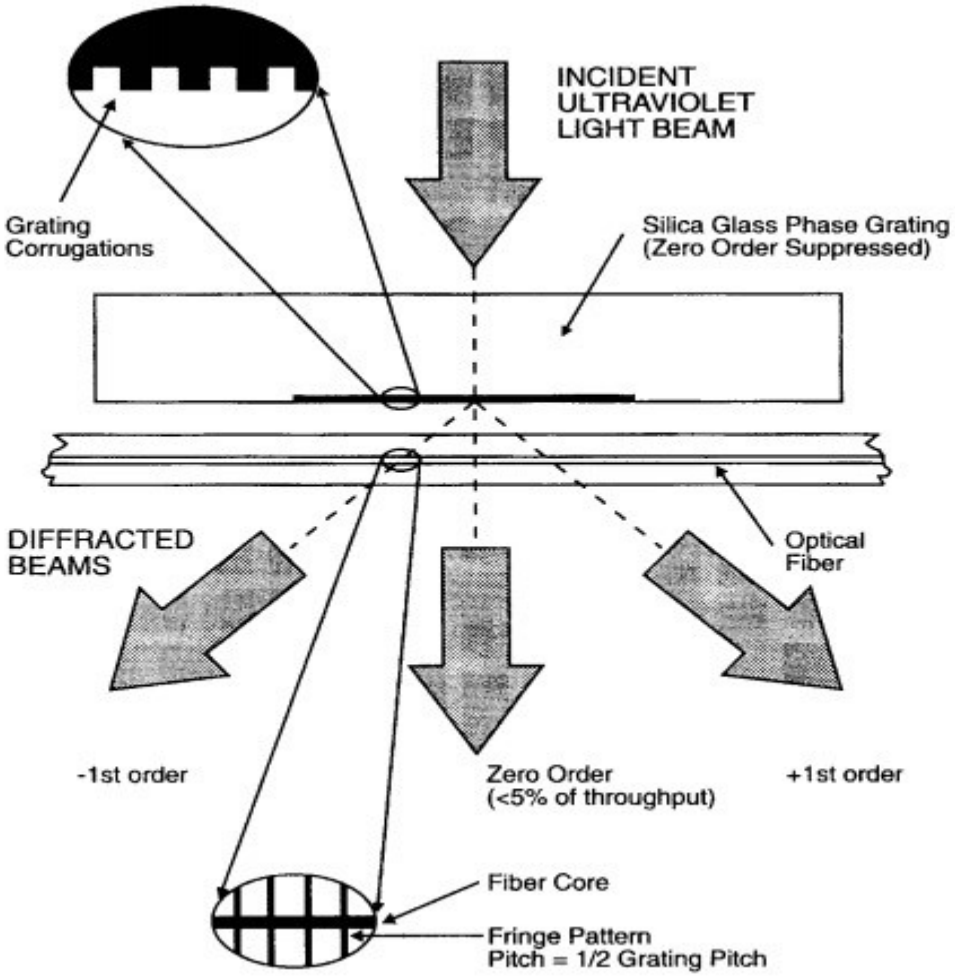

Fig. 2.9 Phase mask technique of optical fiber Bragg grating inscription [35]

2.4.3 Point by point method

Point by point is a method where only one point of the fiber is illuminated by the powerful light source. This point is moved along the fiber through a translator while the intensity of the light is varied to create the difference in refractive index. This approach is great for changing the period, strength and other characteristics of the FBG, but it depends heavily on the precision of the translator.

2.5 Operating principle of the fiber Bragg grating moisture/humidity sensors

In order for any sensor to remain ideally unambiguous in its response, a strictly linear relationship without any hysteresis is required between the sensor output and the measurand. Any deviation from the linearity accounts for the errors and hence needs to be quantified for the sensor or its transfer function. In many instances, the transfer function may deviate from the ideally linear response. The amount of this deviation is determined at the time of calibration.

Sensing with an optical FBG is based on the shift in Bragg wavelength as a function of measurand. In case of optical humidity sensors, the environmental humidity and temperature strongly influence the Bragg wavelength. The grating is artificially made to be humidity responsive by coating the fiber Brag grating with the material that can swell proportionally with respect to the humidity and also has properties like reversibility and high melting point. Combination of an optimum thickness and material properties like hygroscopic coefficient and density are used to linearly relate the external humidity changes to the strain induced on the fiber core and therefore the shift in the Bragg wavelength of the optical FBG.

Figure 2.10 is the pictorial representation of the working of an optical FBG humidity sensor. At a fixed temperature T, the sensor with polymer thickness t_0 shows Bragg wavelength at λ_0, in response to the relative humidity of RH_0%. Increase in humidity from RH_0 to RH_2 % results in the swelling of polymer from thickness t_0 to t_2, which further increases the strain on fiber and red shifts the Bragg wavelength towards higher wavelength ($\lambda_0\ to\ \lambda_2$).

In the same manner, decrease in humidity from RH_0 to RH_1 % desorbs the humidity from polymer reducing its thickness from t_0 to t_1, hence relaxing the strain induced onto the fiber. This shifts the Bragg wavelength towards the lower wavelengths (i.e. $\lambda_0\ to\ \lambda_1$).

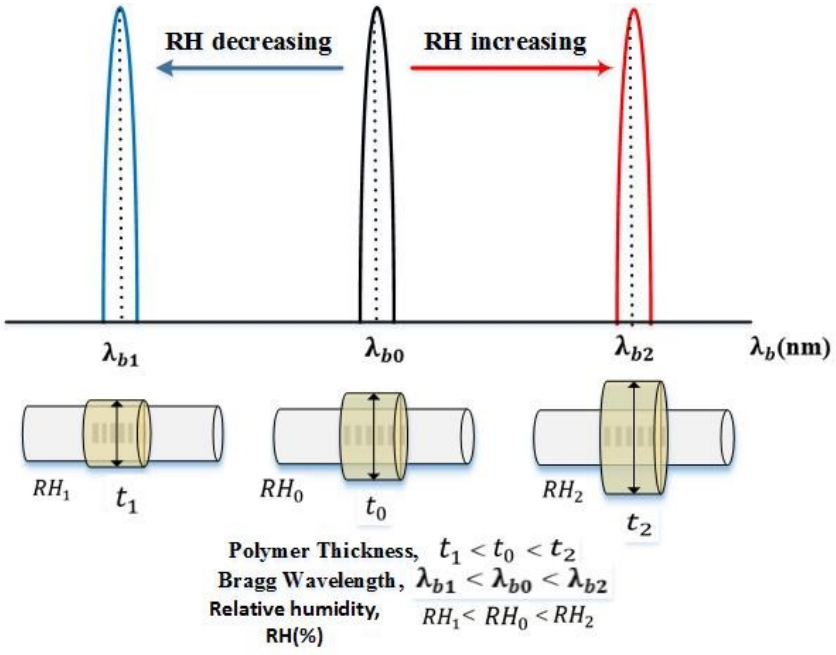

Fig. 2.10 Principle of the operation of the polymer coated FBG humidity sensors

The change in Bragg wavelength for 1 % of RH change determines the sensitivity of the sensor. It is controlled by the composition of the polymer used for coating the fiber and the thickness of that coating.

2.6 Summary

This chapter elaborated the criteria that make optical fiber behave as a waveguide. We discussed the geometry of an optical fiber i.e. core, cladding and the jacket as well as the modes of light propagation through the fiber. Depending on the modes of propagation, two types of fibers are available: Single mode fiber with one signal travelling through the core of small radius and multi-mode fibers with multiple signals travelling through the core of larger radius, bouncing at different angles. Later, we discuss the application of optical fiber as a Bragg reflector. The first order Bragg's condition is defined and the criteria to distinguish various types of Bragg gratings is reviewed. The shift in Bragg's wavelength is a linear function to change in parameters like

temperature, strain and humidity, which is a working principle for many sensors today. Last section discusses the design and working of a humidity sensor using FBG.

3 COMSOL modeling of an optical humidity sensor

3.1 Aim

As mentioned in previous chapter, fiber-optic based humidity sensors can be realized by means of FBG technology and the hygroscopic polymer coating process [1]. Polyimide, a hygroscopic polymer, comes from a class of thermally stable polymers that are often based on stiff aromatic backbones. They demonstrate many excellent mechanical properties, tensile strength, heat resistance and adhesiveness to various substrates. Polyimide resin coated on the FBG sensor once exposed to humidity undergoes a volume expansion, which directly induces axial and radial strain on the FBG. This results in fiber elongation or retraction further leading to the shift in the Bragg wavelength of the FBG sensor. Based on this sensing mechanism, the humidity measurements are carried out by directly reading this wavelength shift through spectrum analysis methods [3-5].
In this chapter, moisture/humidity absorption of polyimide as a function of time is studied using COMSOL multiphysics simulation tool. This model includes transport of diluted species physics to analyze the moisture diffusion into the polyimide-coating layer governed by Fick's law. The concentration of water inside the layer is predicted based on the diffusion coefficient of the coating layer. Swelling of hygroscopic layer induces pressure on fiber, which further results in fiber deformation. This deformation is then studied by a stationary-study in Solid Mechanics interface of COMSOL Structural Mechanics Module as a function of humidity uptake by polymer layer. The effect of polyimide thickness on the induced strain and deformed geometry of the fiber is modeled. The results of the finite element modeling and simulations are used to design and fabricate an FBG optical humidity sensor. The fabricated sensor is tested and its characteristics are reported.

3.2 Simulation of the optical fiber Bragg grating

Flexibility of COMSOL multiphysics simulation tool makes it possible to simulate the behavior of the Fiber Bragg Grating (FBG), design a humidity sensor, analyze mechanical deformation of FBG exposed to hygroscopic polymers and ultimately evaluate electric field strength of

propagating light in FBG as a function of geometric deformation or strain. To start with, desired fiber geometry is created in 2D. After the two-dimensional model is simulated, it is expanded into a three dimensional model to investigate the underlying behavior and characteristics of the optical humidity sensor. Steps shown in figure 3.1 are taken in order to design and simulate a two-dimensional geometric model of a fiber Bragg grating.

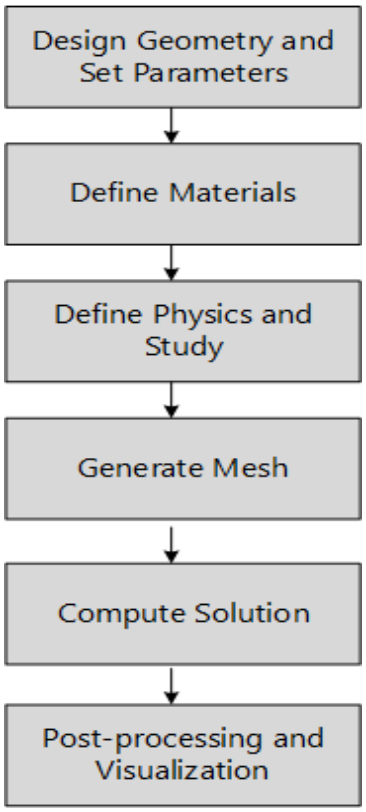

Fig. 3.1 Flowchart of modeling the FBG in COMSOL

3.2.1 Geometry of the optical FBG

Geometric parameters of the fiber used for this model are those of a typical SMF-28 fiber of with core diameter of 8.2 µm and cladding diameter of 125 µm. For the ease of computing and visualizing, the length of fiber is kept 5mm in the basic model. An array of fringes is used to design the geometry of the grating. For model simplicity, number of fringes is limited to 200 with the grating period (Λ) of 0.513 µm. A view of 2-D fiber geometry in the model is given in figure 3.2.

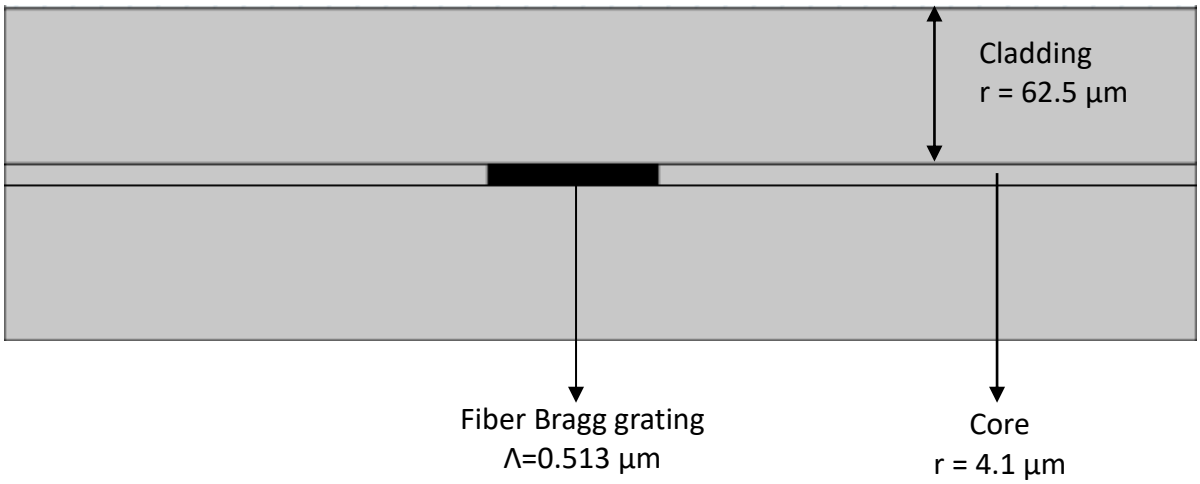

Fig. 3.2 A 2-D geometric representation of a FBG in COMSOL

All geometric components are grouped into three separate domains, each one for the core, cladding and the grating. The material properties of each of these are defined in the *Materials* section. The *Materials* section provides the flexibility needed to design the models using a combination of existing material properties (from the material library in COMSOL) as well as manually defined properties. The Young's modulus, Poisson's ratio and density of silica glass are predefined in the materials library. Refractive index of the core and cladding are manually defined as 1.50 and 1.488 respectively.

3.2.2 Physics behind the modeling of the optical FBG

Wave propagation in the fiber is analyzed using *electromagnetic waves interface* of *wave optic module*. Light propagation, transmitted wavelengths and the reflected wavelength are simulated based on Snell's and Fresnel's laws and none of the Bragg equations and expressions is predefined in the model. *Ports* are defined at the fiber endings to characterize the boundary where electromagnetic wave enters and exits the fiber. This ultimately defines the direction of wave propagation inside the fiber. Activated excitation is selected for port 1 which signifies the end from which the wave is launched. An unexcited port 2 is added at the other end of the core and cladding to signify the end where light would leave the fiber. COMSOL uses Wave equation, electric (equation 3.1) and perfect electric conductor (equation 3.2) to spatially solve electric field inside the fiber. These equations are given as

$$\nabla \times (\nabla \times E) - {k_0}^2 n^2 E = 0 \tag{3.1}$$

$$n \times E = 0 \tag{3.2}$$

where, E is the electric field, k_0 is the wave number of free space and n refers to the refractive index.

Finite Element analysis using COMSOL is a heavily mesh dependent analysis. Meshing refers to the subdivision of the mathematical model into (close to infinite) small, non-overlapping components, called elements. The response of the whole model is computed by assembling the computations on each of the individual element of the mesh. Optimum mesh refining is very necessary for precise modeling in COMSOL. If the mesh size is too large, the simulation results have tendency to be erroneous. On the other hand, if the mesh size is too small, the model requires higher memory and time for computation.

Since electromagnetic wave spatially varies with respect to the wavelength, the meshing of this model should be in the range of fractions of wavelength. On testing various meshes in this model, it is found that the electromagnetic wave physics works best with the mesh element size of λ/5 nm or lower. Since the computations at the regions containing the core and grating require even more precise calculation of the electric field, mesh element size is further reduced to λ/10 nm at these regions. Figure 3.3 shows the mesh distribution inside the model. It can be observed that the mesh of the core and grating domains is much finer than that of the cladding domain.

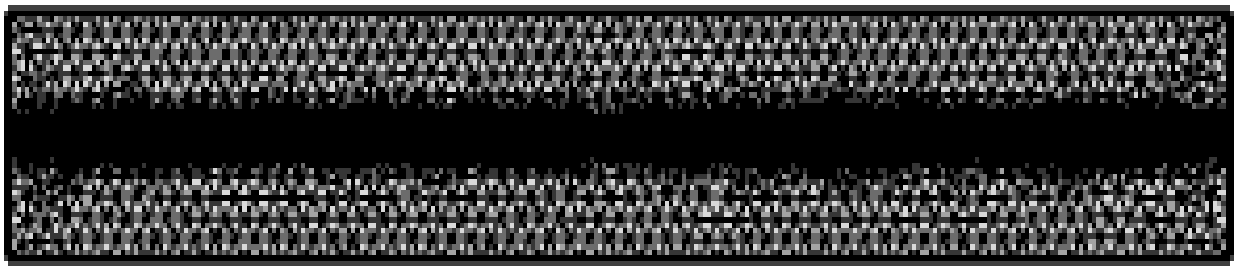

Fig. 3.3 Mesh distribution inside the fiber geometry in COMSOL. Mesh size is kept finer at the core and grating domains than the cladding domain

3.2.3 Study and the analysis of the designed optical FBG model

A study is selected for each model, which implies to the solver that would be used in the simulations. A combination of three types of analyses is used to compute this model. *Boundary mode analysis* is used to compute the propagation constants or the wave numbers for a given

frequency at a port. Two-boundary mode analysis is done in this model, each one for the port 1 and 2 (defined in section 3.2.2). Boundary mode analysis study step at a port/boundary is combined with a *frequency domain* study step, which is used to obtain the transmission or reflection characteristics of the model v/s frequency range. Frequency and wavelength are related by

$$f = \frac{c_0}{\lambda} \tag{3.3}$$

where f is the frequency, c_0 is the speed of light in the vacuum and λ is the vacuum wavelength. A wavelength domain study step is used to compute the grating structure transmission and reflection characteristics with respect to the wavelengths. The range of wavelengths is specified as 1520-1620 nm in this study step to limit the solver to perform the computations in specific range of wavelengths and hence frequencies.

3.2.4 COMSOL simulation results for a 2D model of the optical FBG

COMSOL provides several tools for post processing and analyzing the simulated results. This section discusses the detailed simulations results obtained from the 2D modeling of the optical FBG in COMSOL. Figure 3.4 shows the electric field distribution inside the geometry of model using the range of colors where red represents the areas inside the geometry with highest electric field values and the blue represents the area with lowest electric field values. An interference pattern of high and low electric fields can be seen in the figure, which symbolizes the reflected wavelength at Bragg wavelength.

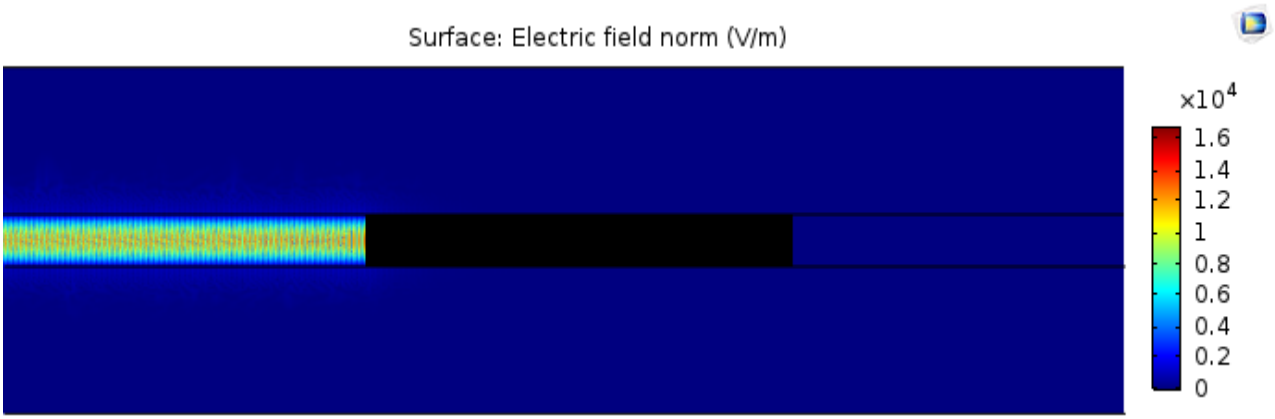

Fig. 3.4 Electric field strength of travelling wave inside the FBG at the Bragg wavelength[36]

Transmission and reflection characteristics of fiber are obtained using *1 D plot group* from the *results* section. An expression is defined in the global plots as 'ewfd.S11d' (to call the reflection characteristics from scattering matrix in the solver or S21 for transmission characteristics) is selected to be plotted with respect to the wavelength range from 1520 nm to 1620 nm. The resulting plot is shown in figure 3.5. It can be noted that a reflection peak is obtained around 1540 nm wavelengths. It satisfies the Bragg resonance condition ($\lambda_b = 2\, n_{eff}\Lambda$) hence proving the basic FBG model COMSOL to be legit and reliable. FWHM of grating obtained in this simulation result is large because the length of grating used is very small (i.e. 200 $fringes \times 513\ nm$).

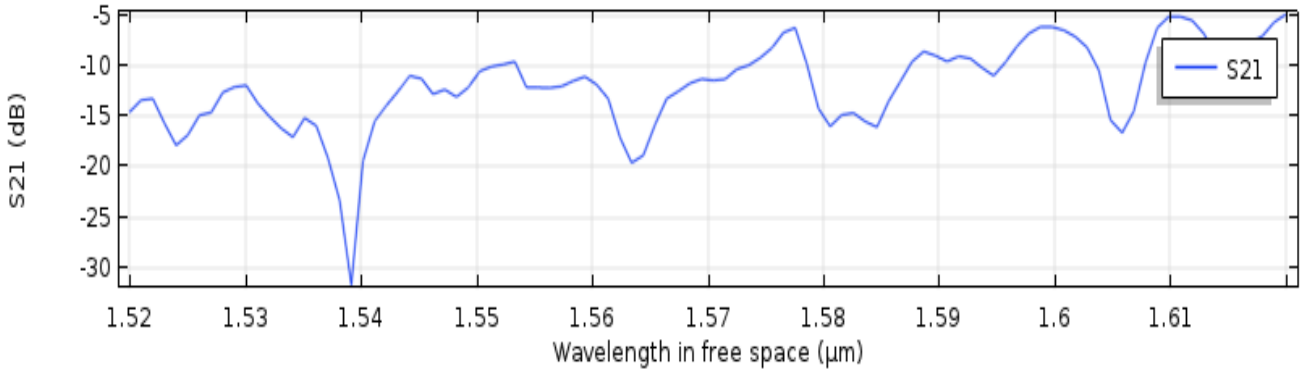

Fig. 3.5 Reflected wavelength plot of the grating. It shows the Bragg wavelength position at about 1.54 μm

3.3 Design of the optical humidity sensing element

In the above section, a fundamental structure of an optical Fiber Bragg grating is simulated. A constructive and destructive interference of electric field components were observed in the core region of the fiber. Reflection spectrum of the grating was simulated with respect to the wavelength swept over a range.

In this section, humidity is converted into an indirect source of stress onto fiber core. This is done by coating the fiber with a thin layer of humidity sensitive hygroscopic material. On increasing the humidity concentration, the material swells up upon absorption and exerts the stress on core of the fiber whose value in real time is simulated using COMSOL structural mechanics module. The

alterations in the electric field pattern inside the core are finally studied to predict the reflected Bragg wavelength shift and hence the sensor behavior. The design of humidity sensor is explained as follows.

3.3.1 Geometry of the humidity sensor in 2D

FBG Humidity sensor model uses the geometry of optical fiber simulated in section 3.1. It is a 2-dimensional structure with core and cladding diameter of 8.2 μm and 125 μm respectively. Two rectangles of height 10μm are constructed on either side of cladding along the grating length. In order for this fiber to behave as a humidity sensor, these rectangles should function as a hygroscopic material coating around the fiber. This can be done by assigning Polyimide as the coating material from the materials library.

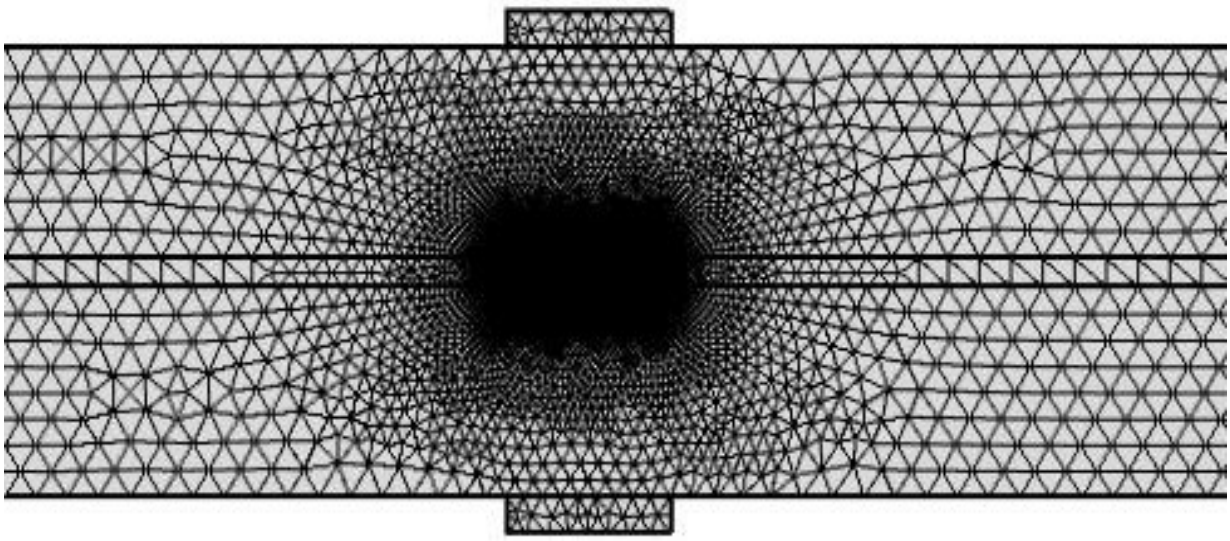

Fig. 3.6 Geometry and the mesh distribution of the optical humidity sensor in 2D COMSOL model.

The properties of the fiber and coating in the *Materials* section are given in table 3.1.

Property	**Fiber**	**Coating**
Young's Modulus	78×10^{10} Pa	3.1×10^{9} Pa
Poison's ratio	0.17	0.34
Density of the material	2203 kg/m^3	1300 kg/m^3

Table 3.1 Material properties of the fiber and the polyimide coating used for modeling the humidity sensor in COMSOL 2D.

3.3.2 Physics behind the modeling of the humidity sensor

In the *Physics s*ection, *Solid Mechanics* interface of the *Structural Mechanics* module is used to analyze the deformation, stress in the geometry of FBG. To study internal stress and strain caused by changes in humidity content, *hygroscopic swelling* is selected in this section. The domain containing the coating is selected as the hygroscopic material. The coefficient of hygroscopic swelling ($1.1 \times 10^{-4} m^3$/kg) is extracted from the properties in the material library. Molar mass of water 0.018 kg/mol is used as the *fluid molar mass*. Strain reference concentration of 0 mol/cc is set as initial boundary condition in the model. This value determines the concentration at which there is no stress/strain due to hygroscopic swelling of the coating. In this simulation the outermost boundaries of both coatings are considered as fixed constraint boundary so the swelling material is only expanded toward the fiber.

3.3.3 Study and the analysis of the designed humidity sensor

Due to heavy meshing requirements of electromagnetic wave interface, the model is simulated in two steps. Firstly, the stress experienced by the grating upon swelling of polymer is used to trace

the geometric deformations of the structure. The *stationary study* is used to compute this physics. In the second step, this deformed geometry is exported to the coordinate system of Electromagnetic Waves interface. This is done using *re-mesh deformed configuration* in COMSOL. Hence the deformed structure is re-meshed in boundary mode analysis, frequency and wavelength domain studies to calculate the electric filed strength in the deformed fiber.

3.3.4 COMSOL simulation results showing the behavior of the humidity sensor

Hygroscopic swelling of polyimide layer results in deformation of geometry of fiber. The deformation and stress values inside the FBG structure after exposing to 1mol/cm3 humidity concentration are shown in Figure 3.7. Expansion of polymer walls can be clearly distinguished from the original geometry in the figure. Stress values are displayed in the range of colors where red is the area of maximum stress value and blue is the area of minimum stress experienced inside the structure. Since the coating is placed exactly on top of the grating, higher amounts of stressed are seen under that area than the ends of the fiber.

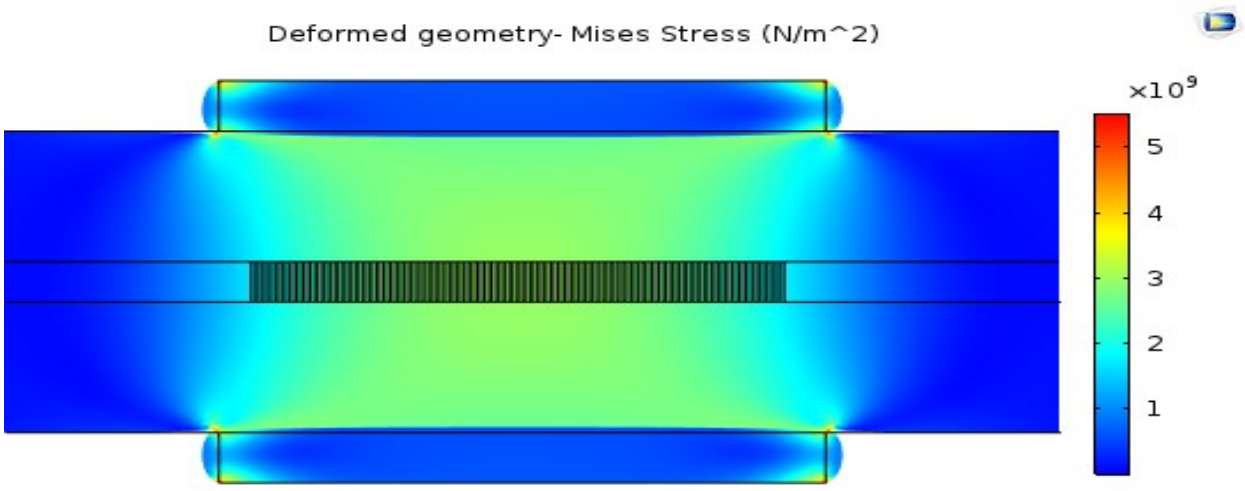

Fig. 3.7 Deformed geometry and stress values experienced by FBG after exposing to 1mol/m3 humidity concentration at constant temperature[36]

The stress on grating produce changes in the geometry of grating so minute that they aren't visible in the drawings. However while meshing at mesh object size as minimum as 10^{-9}m, COMSOL detects the changes in grating geometry. The effect of this deformation on electric field pattern in

electromagnetic wave physics is determined in results of this model. Figure 3.8 a, b &c shows the electric field inside the structure when the concentration of humidity in the environment around it is 0.01, 0.5 and 1 mol/m3 respectively. It can be clearly seen that the electric filed penetrates into the cladding with increase in humidity around the sensor. As the stress is increased, the strength of electric field inside the core is reduced. The range of colors show the amounts of electric field where red denotes for the higher field and blue for the lowest field value.

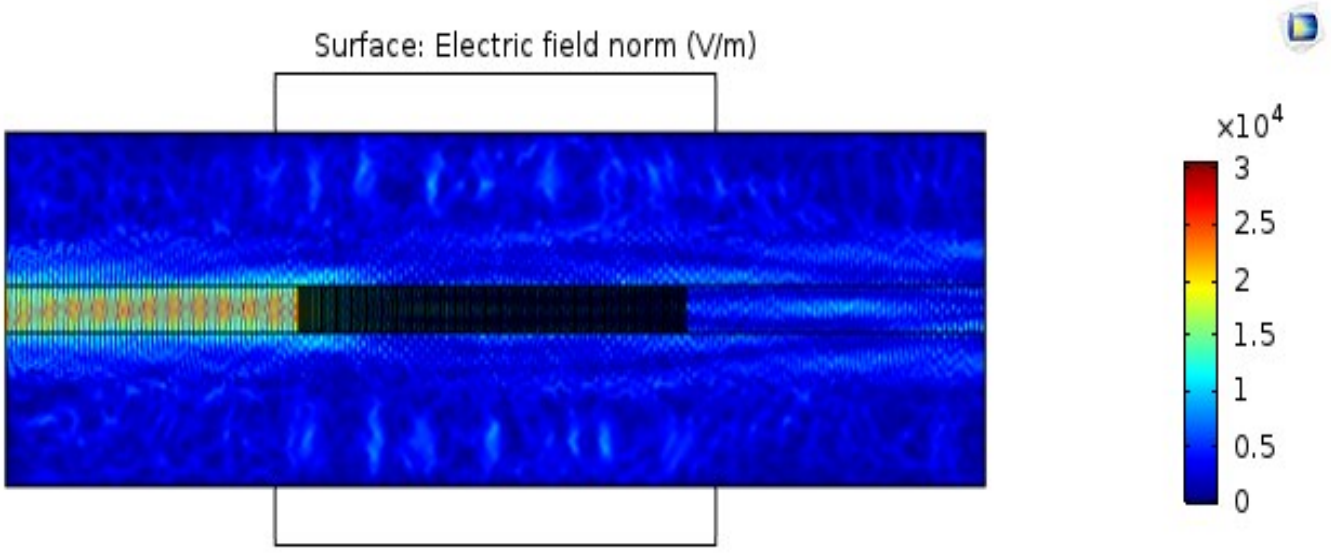

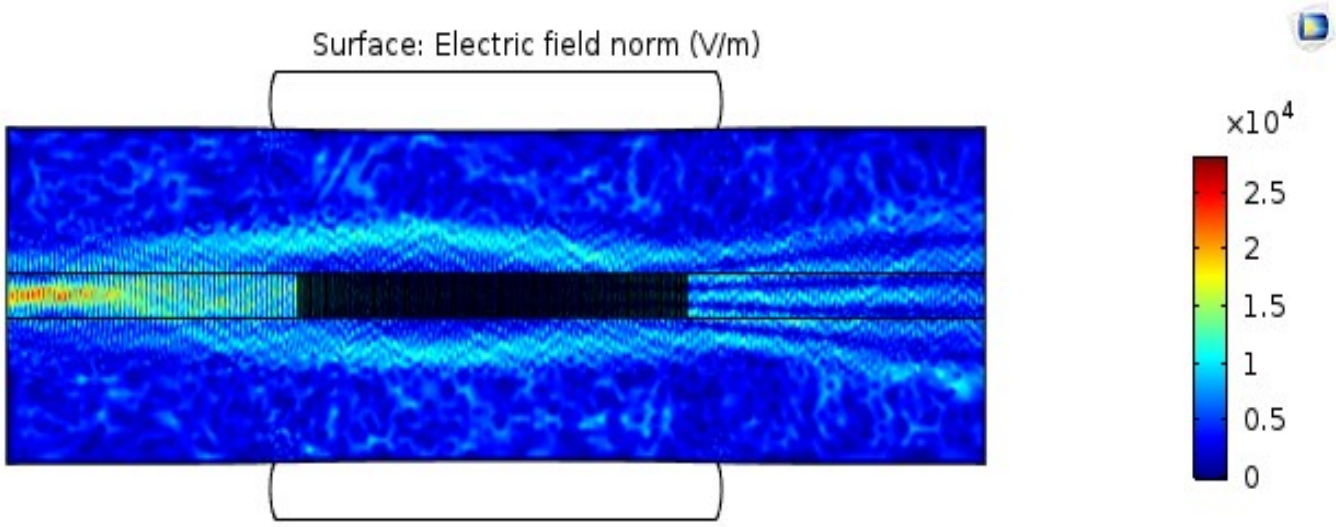

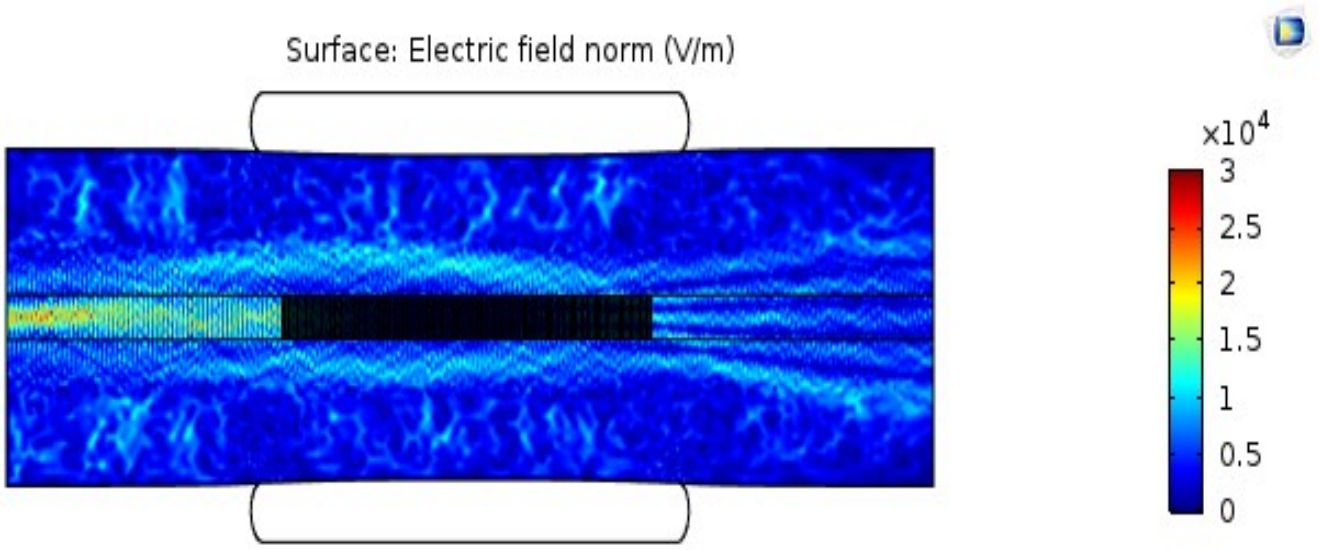

Fig. 3.8 Electric field distribution in the fiber deformed with the humidity concentration of **a)** 0.01 mol/ m3, **b)** 0.5 mol/ m3, **c)** 1 mol/ m3[36].

Reflection characteristics of the deformed structures shown above are summarized in table 3.2. It is observed that the Bragg wavelength moves towards higher wavelength when the grating is under stress induced through humidity. Graphical representation of wavelength shift v/s humidity concentration is given in figure 3.8. Clearly, we can comment high linearity in the sensor behavior in the presence of humidity.

Humidity concentration (mol/ m3)	0.01	0.5	1
Reflected wavelength (nm)	1539.2	1540.03	1541
S21 (dB)	-30	-26	-30

Table 3.2 Shift in Bragg wavelength of the deformed FBGs with respect to different humidity concentrations.

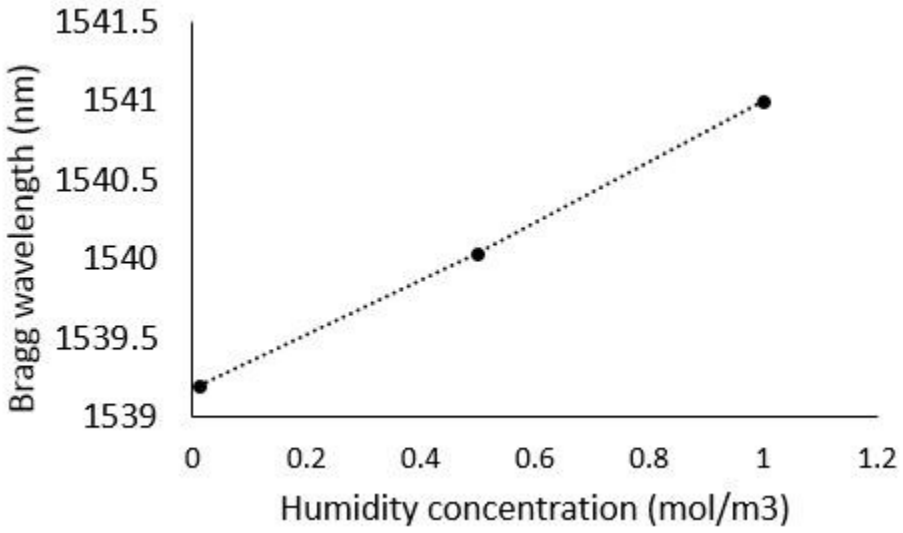

Fig. 3.9 COMSOL result showing high linearity in the Bragg wavelength shift of humidity sensor while increasing humidity concentration.

Sensor shows linear behavior with respect to humidity concentration, which proves the authenticity of model. However, the fixed boundary constraints required in COMSOL assumes the outer boundary of polymer to be fixed. This exerts the maximum stress towards the polymer-cladding interface. The model requires the need to find a way to satisfy fixed boundary condition without affecting the working of sensor. Moreover, the claims about sensitivity and response time of the sensor cannot be made just yet because of its 2 dimensional geometry. In order to resolve these concerns, a new three-dimensional model of sensor is prepared. This model concentrates on predicting the influence of coating on working of the sensor. It elaborates the mechanism of humidity absorption and mass uptake by the polyimide layer, response time of the sensor and the stress exerted on the core during this process.

3.4 Study of the effect of the polymer coating on the sensor behavior

This section contains a 3-dimensional analysis of polymer coated optical humidity sensor with three different layer thicknesses of polyimide. This study is helpful in studying the mechanism of

diffusion into the polymer until the saturation of mass up taken thus determining the response time of the sensor.

3.4.1 Geometry of the polymer coated optical humidity sensor in 3D

The geometry considered for the simulation is a 3 dimensional cylindrical optical fiber with 125μm and 8.2μm cladding and core diameters respectively. The fiber has a 24mm length and is coated with a polyamide layer, initially 20μm thick throughout its length as shown in figure 3.10.

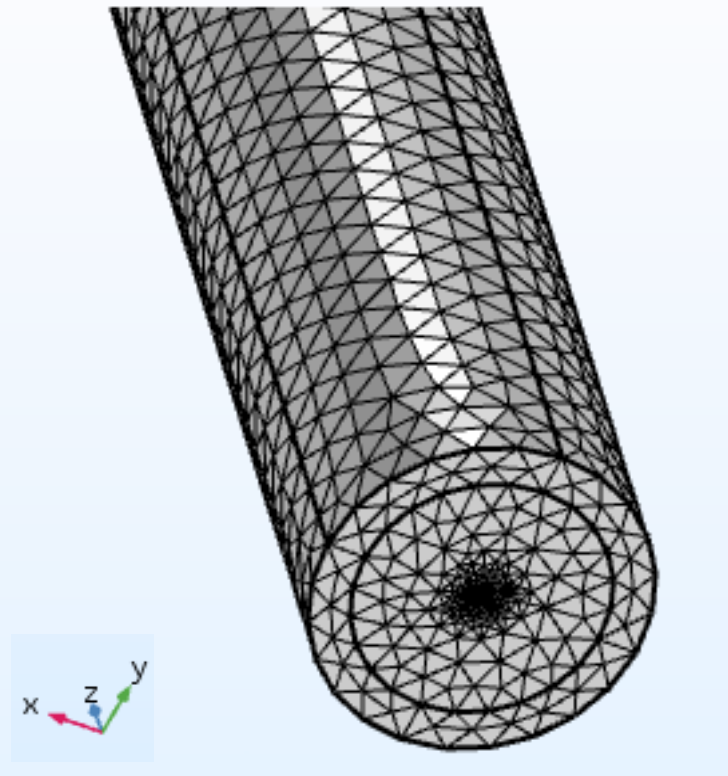

Fig. 3.10 Cross section of a polyimide coated fiber in COMSOL 3D model. The triangular elements on the boundary are the mesh used during the simulations.

3.4.2 Physics behind the modeling of the coating for the optical humidity sensor

The model includes transport of diluted species physics (tds) to compute variation of humidity concentration in hygroscopic polyimide-coating layer. The concentration of water inside the hygroscopic layer is predicted based on a time-dependent isotropic diffusion, which follows Fick's law. Since the sensor is assumed to be inside an infinitely large chamber, the diffusion is considered to start from a constant source. The concentration boundary condition with constant

moisture concentration over time is applied to all external boundaries of the polymer to show the relative humidity around the fiber.

Absorbed water swells up the hygroscopic polymer layer and induces deformation in coating layer, which results in strain on fiber. COMSOL Structural Mechanics Module is used to model the stress that the fiber is experiencing. The central axis of the fiber is considered as a fixed constraint boundary condition. Since deformation is impossible on this boundary, it induces stress inside the structure. All around the polyimide coating is considered free boundaries, which induces deformation of the structure by swelling.

3.4.3 Study and the analysis of the 3D-optical humidity sensor

To compute the time varying deformation induced varying stress due to diffusion of moisture into polyimide, *time dependent study* is used in the model. In study settings, the limiting range of time for the study is specified from 0 to 10 minutes. This is done so that the time dependent solver solves the movement of water and the structural deformities from start till 10 minutes. *Stationary study* is added as the second study in order to see stress and strain. The computations are carried out and the results are listed in the section below.

3.4.4 COMSOL simulation results on the effect of the coating on the humidity sensor

COMSOL shows the stages of moisture diffusion in polymer layer at any point from 0 to 10 minutes. Figure 3.11 shows the state of moisture diffusion into a 20 μm polymer layer when it is exposed to 20% RH at 2nd minute. Moisture concentration profile (mol/m3) is shown in cross sections of the fiber along XZ and XY planes. Red color signifies the highest moisture concentration while the blue denotes the lowest concentration. The figure illustrates the movement of moisture from an area of high concentration (air-polymer boundary) to an area of low concentration (polymer-cladding boundary). A similar study is conducted for the polymer layer thickness of 10 and 30 μm too. The results show that the diffusion reaches a saturation point after a certain time, which is a function of the thickness of the polymer.

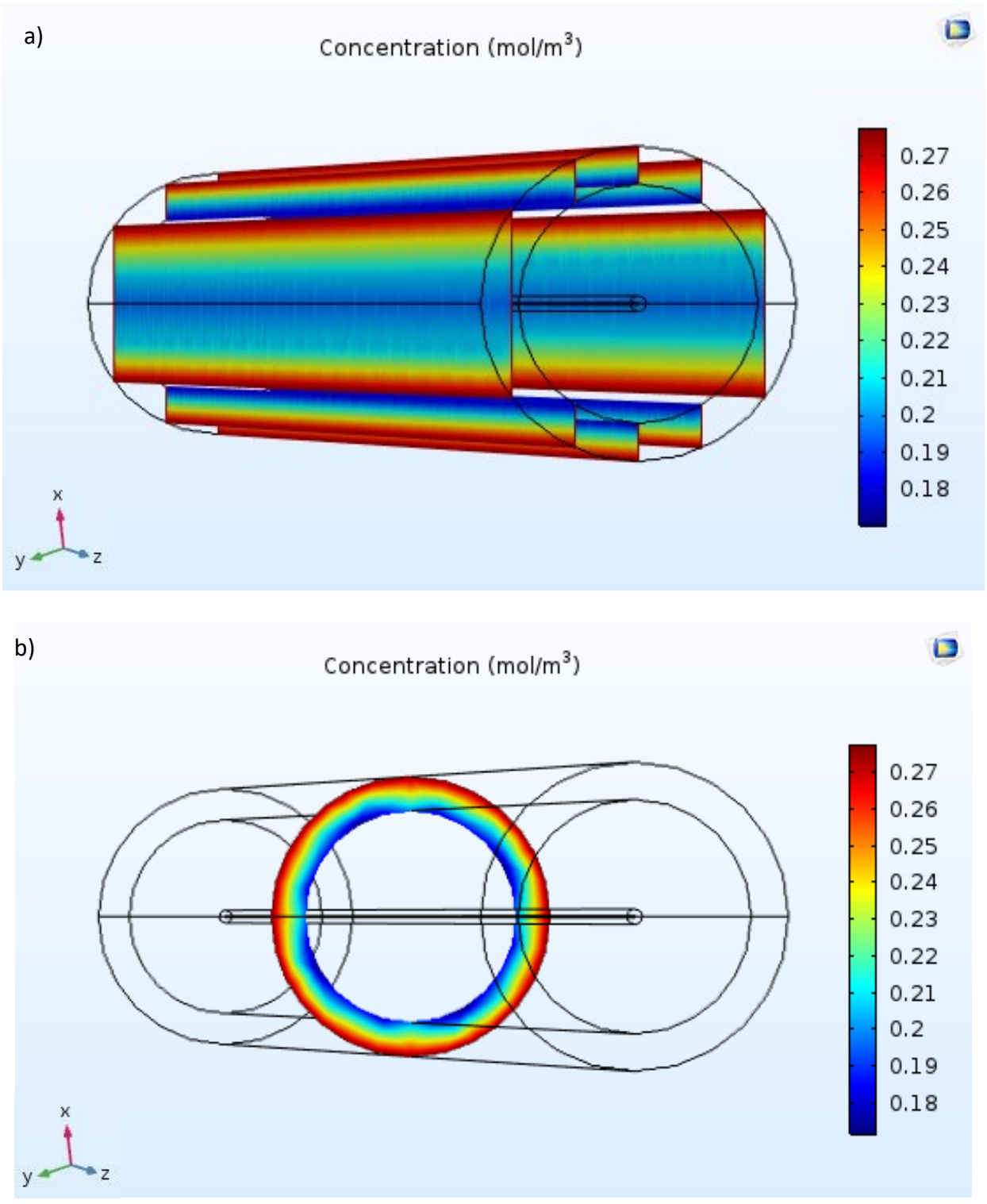

Fig. 3.11 Moisture concentration (mol/m3) inside the polymer layer simulated by COMSOL Transport of Diluted Species (tds). In 20%RH, after 2 minutes, moisture has partially diffused into the layer **a)** XZ- plane slices**, b)** XY-plane slice.

COMSOL simulation graphs showing the trend of the moisture absorption which is based on cumulative mass of water inside the polymer layer is given in figure 3.12. Simulations are repeated for 10, 20 and 30 µm of polymer layer thicknesses, in 20% and 50% RH. It is seen that the diffusion reaches the saturation region after 2, 9 and 20 minutes for 10µm, 20µm and 30µm polymer layer thicknesses respectively. So, at a constant temperature, the saturation time depends on polymer thickness and is independent of the surrounding moisture concentration.

a)

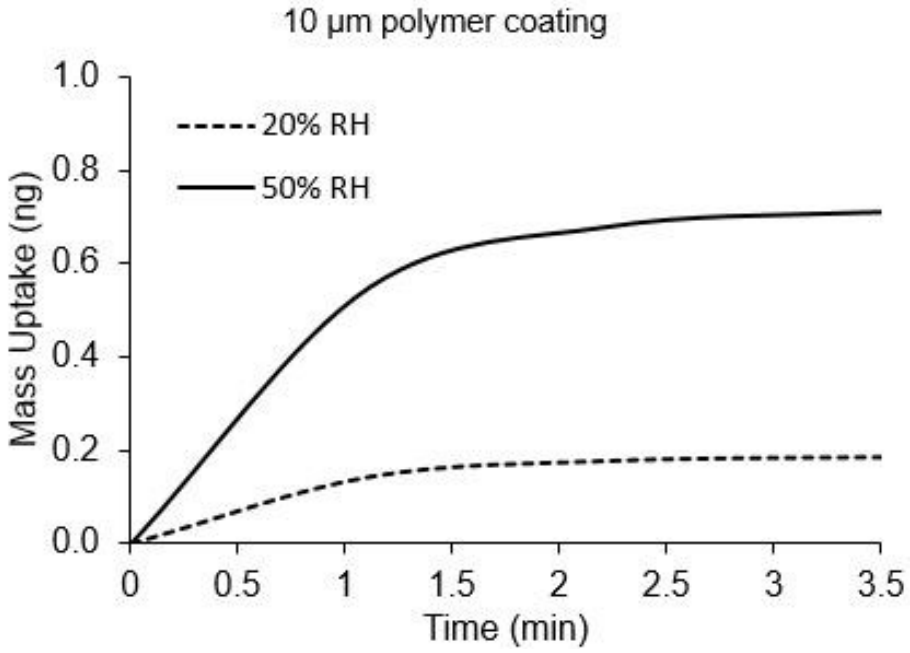

b)

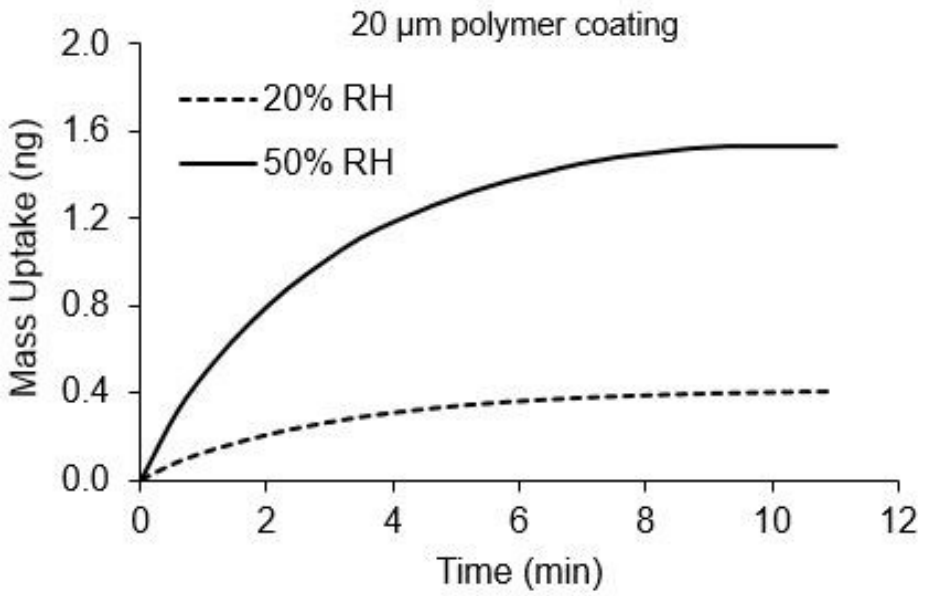

c)

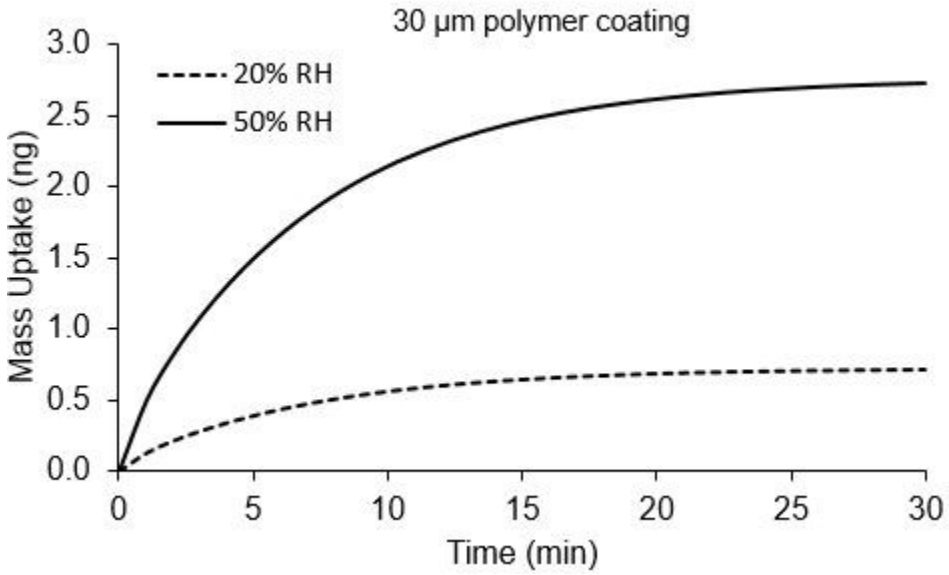

Fig. 3.12 Water mass uptake vs time graph shows that the saturation point is a function of polymer thickness. **a)** after 2 minutes for the layer of 10 µm, **b)** after 9 minutes for the layer of 20 µm and **c)** after 20 minutes for the layer of 30 µm.

Figure 3 shows the Mises stress (3D state of the stress or stress field) along the cross section of the fiber, when the moisture absorption in polymer reaches the saturation stage in the case of 20% RH. The figure demonstrates the distribution of the stress in polymer with various thicknesses. As

it can be seen from the figure, regardless of the thickness, the stress is distributed uniformly all around the fiber and it is exerted from all directions toward the core of the fiber. It is maximum at the cladding surface in contact with polymer and then decreases with respect to distance as we move towards the core. Our observations also show that the thicker polymers exert larger stress on the core of the fiber.

a)

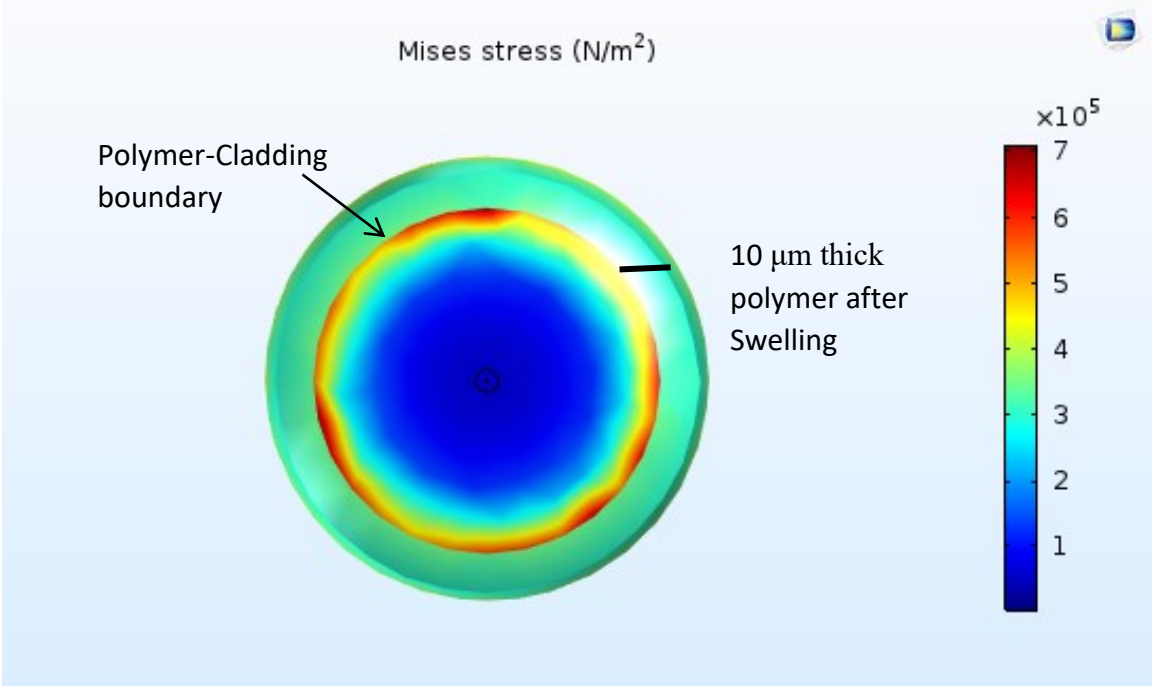

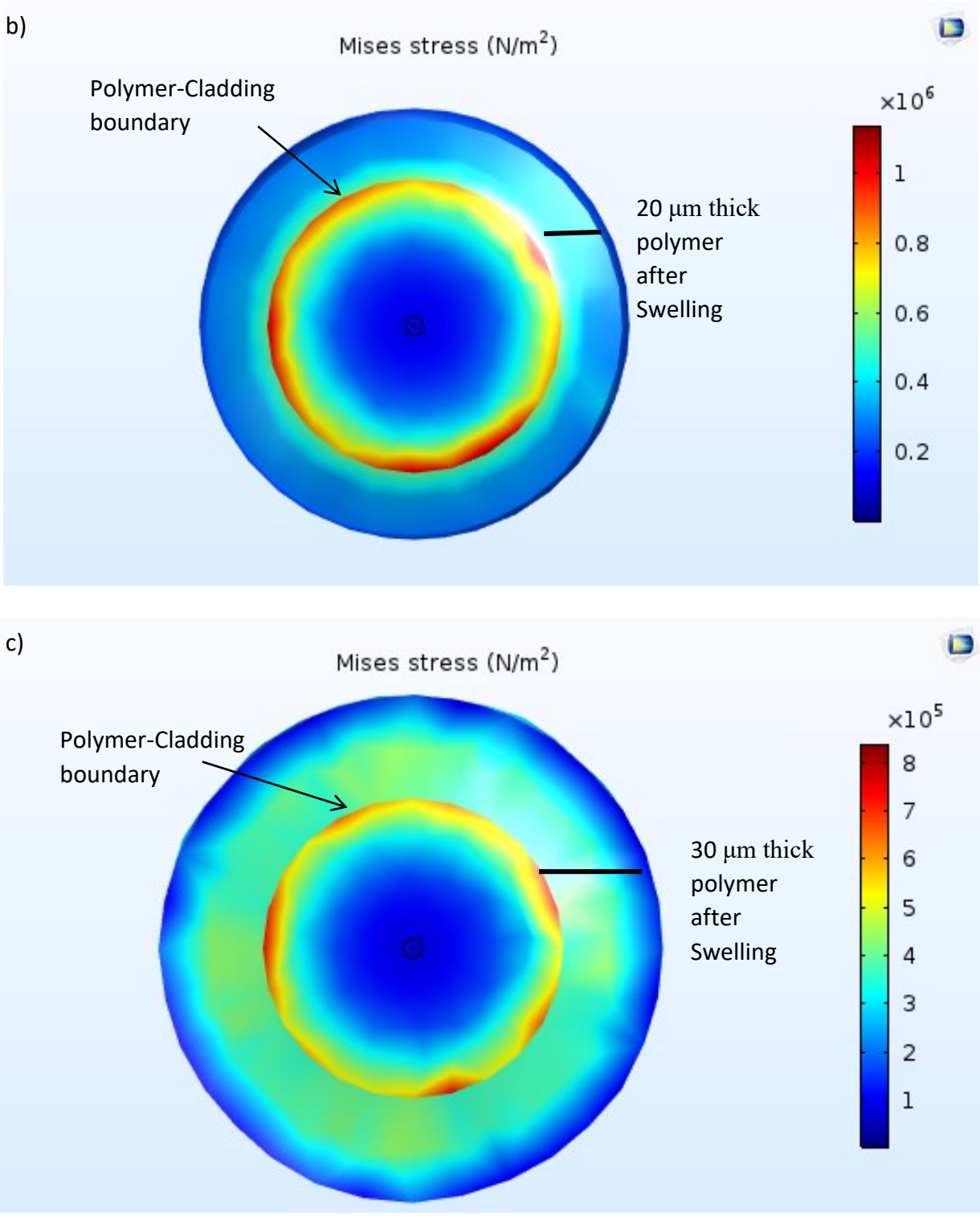

Fig. 3.13 Distribution of Mises stress along the cross section of the fiber when the humidity absorption reaches the saturation stage for **a)** 10 µm, **b)** 20 µm, and **c)** 30 µm of polymer[37].

3.5 Summary

This chapter outlined a step by step design, simulations and working of an optical humidity sensor. Moisture transportation throughout the polyimide coating shows that the moisture absorption in polymer layer reaches a saturation point, which depends on the thickness of the polymer. Water mass uptake by polymer with respect to time is also calculated. Our studies show that due to the volume expansion/contraction of the polymer a uniform and reversible force is exerted on the fiber. As the thickness of the polymer increases, the penetration depth of the stress into the cladding increases.

4 Modeling of the optical humidity sensor in MATLAB

4.1 Aim

Chapter 3 plays a pivotal role in choice of the material to be used for coating the sensor. Properties of the coating material like its thickness and the coefficient of hygroscopic expansion decides the response time of the sensor. Based on the simulation results, a 24 mm polyimide coating was chosen to be tested in the laboratory for humidity sensing application.

In this chapter, the spectral signal of the sensor is studied and simulated in MATLAB. The goal is to achieve a clear and sharp spectrum with high transmission and free from noises and side lobes. In order to achieve this, different types of apodization techniques are tested. Finally, a suitable size and apodization combined with the coating properties extracted from COMSOL are used in fabrication of the humidity sensor. The sensor is then tested in the laboratory for its behavior.

4.2 Theoretical background

4.2.1 Refractive index perturbations along the fiber length

When laser irradiation is scanned through interferometric, point-by-point or phase mask technique along the length of an optical fiber, permanent refractive index perturbations, $\delta n_{eff}(z)$, are induced into the core of the fiber. These perturbations are permanent in the sense that they last for decades given the fiber after UV exposure is heated for a few hours at a temperature of 50°C above its maximum operating temperature. The induced refractive index perturbations are represented mathematically by the following equation[38].

$$\delta n_{eff}(z) = \overline{\delta n}_{eff}(z) \cdot \left\{1 + v \cdot \cos\left[\frac{2\pi}{\Lambda} z + \varphi(z)\right]\right\} \tag{4.1}$$

where v is the fringe visibility of the index change, $\phi(z)$ denotes the grating chirp, Λ is the grating period given by $\Lambda = \lambda/2 \cdot n_{eff}$, λ is the Bragg wavelength and n_{eff} is the effective refractive index, $\overline{\delta n}_{eff}(z)$ is the modulated refractive index profile as a function of grating length z (apodization profile) and it is given by

$$\overline{\delta n}_{eff}(z) = \overline{\delta n}_{eff} \cdot f(z) \tag{4.2}$$

where $\overline{\delta n}_{eff}$ is the peak to peak refractive index modulation and $f(z)$ is the apodization function.

4.2.2 Scope of the apodization function

Uniform Bragg grating has a finite periodically varying rectangular structure. The optical response of the grating is obtained through the Fourier transform, which for a rectangular function is a sinc function with multiple side lobes. Matsuhara et al. [39] proposed that as a result of a slowly varying coupling coefficient along the length of the coupling region (grating length), it is possible to design the band–rejection filters with very low side lobes. This concept of suppression of the side lobes in the spectrum by varying the refractive index change is termed as apodization. A functional shape is provided to the profile of the index modulation along the grating length, which creates a non-homogeneous fringe pattern. Various apodization techniques have been investigated and compared in literature, among which Gaussian provides the best performance in terms of the side lobes suppression[40]. Following is the list of profiles generally used for apodization[40], [41]

1. Gaussian

$$f(z) = \exp\left(-4\left(\frac{z-\frac{L}{2}}{\frac{L}{3}}\right)^2 \ln 2\right) \tag{4.3}$$

2. Raised Sine

$$f(z) = sin^2\left(\frac{\pi z}{L}\right) \tag{4.4}$$

3. Hamming

$$f(z) = 0.53 + 0.46cos\left(\frac{\pi(z-\frac{L}{2})}{L}\right) \tag{4.5}$$

4. Nuttall

$$f(z) = a_0 - a_1 cos\left(2\pi\left(\frac{z}{L}\right)\right) + a_2 cos\left(4\pi\left(\frac{z}{L}\right)\right) - a_3 cos\left(6\pi\left(\frac{z}{L}\right)\right) \tag{4.6}$$

The modulation of refractive index plays an important role in reflectivity, bandwidth and side lobe suppression. Reflectivity and bandwidth of the optical signal will increase as the refractive index modulation increases, whereas, the side lobe suppression degrades with increasing of index modulation. So an optimum range of refractive index modulation has to be determined in order to maintain the quality of signal.

4.2.3 Coupled mode theory

A simple solution for spectral profile of the grating is obtained using Coupled mode theory (CMT). CMT is the most widely used tool for analyzing the grating structures [42], [43]. Any irregularity or perturbation in the refractive index of an optical fiber produces coupling and energy exchange between the modes[44], [45]. Light is reflected due to coupling between two counter directional modes inside the core at the Bragg's condition. So at any instant, t, the electric field inside the core, $\vec{E}(x, y, z, t)$, is given as the linear combination of the forward propagating field, $\overrightarrow{E_b}(x, y, z, t)$, and the backward propagating field, $\overrightarrow{E_a}(x, y, z, t)$ [46].

$$\overrightarrow{E_b}(x, y, z, t) = \sum_{l_p=0}^{(l_p)max\,-\,1} \sum_{m_p=1}^{(m_p)max} B_{l_p m_p}(z) \times$$

$$exp\left[i\left(\omega t - \beta_{l_{pm_p}} z\right)\right]\left(\vec{e}^{\,t}{}_{l_p m_p}(\mathrm{x,y}) + \vec{e}^{\,z}{}_{l_p m_p}(x, y)\right) \tag{4.7}$$

$$\overrightarrow{E_a}(x, y, z, t) = \sum_{l_q=0}^{(l_q)max\,-\,1} \sum_{m_q=1}^{(m_q)max} A_{l_q m_q}(z) \times$$

$$exp\left[i\left(\omega t - \beta_{l_{qm_q}} z\right)\right]\left(\vec{e}^{\,t}{}_{l_{qm_q}}(\mathrm{x,y}) + \vec{e}^{\,z}{}_{l_{qm_q}}(x, y)\right) \tag{4.8}$$

where $\beta_{l_{pm_p}}$ and $\beta_{l_{qm_q}}$ are the wave propagation constants of the modes $p(LP_{l_pm_p})$ and $q(LP_{l_qm_q})$ respectively; l_p and m_p are the p_{th} mode's azimuthal and radial order; l_q and m_q are the q_{th} mode's azimuthal and radial order; $\vec{e}^{\,t}{}_{l_pm_p}$ and $\vec{e}^{\,z}{}_{l_pm_p}$ are the transverse and longitudinal component of the electric field associated to the mode $p(LP_{l_pm_p})$ before the grating inscription. $\vec{e}^{\,t}{}_{l_qm_q}$ and $\vec{e}^{\,z}{}_{l_qm_q}$ are respectively the transverse and longitudinal component of the electric field associated to the mode $q(LP_{l_qm_q})$ before grating inscription; ω is the light pulsation; $B_{l_pm_p}$ and $A_{l_qm_q}$ are the amplitudes of the backward and forward electrical fields respectively of the modes $p(LP_{l_pm_p})$ and $q(LP_{l_qm_q})$.

In the most guided mode i.e. LP_{01} of the reflection FBG, the coupling of the forward propagating mode with electric field, $\overrightarrow{E_p}(x,y,z,t)$, to the counter propagating mode of electric field, $\overrightarrow{E_q}(x,y,z,t)$, is governed by the coupled mode equations as follows

$$\overrightarrow{E_p}(x,y,z,t) = B(z)\, exp[i(\omega t - \beta z)](\vec{e}^{\,t}(x,y) + \vec{e}^{\,z}(x,y)) \tag{4.9}$$

$$\overrightarrow{E_q}(x,y,z,t) = A(z)\, exp[i(\omega t - \beta z)](\vec{e}^{\,t}(\mathrm{x},\mathrm{y}) + \vec{e}^{\,z}(x,y)) \tag{4.10}$$

The presence of grating signify the dielectric perturbations which cause the modes to be coupled such that the mode of amplitude $A\,(z)$ and an identical counter-propagating mode of amplitude $B\,(z)$ evolve along the z axis as

$$\frac{d\mathrm{A}(z)}{dz} = i\kappa B(z)\exp[-2i(\Delta\beta)z] \tag{4.11}$$

$$\frac{dB(z)}{dz} = i\kappa^* A(z) \exp[2i(\Delta\beta)z] \tag{4.12}$$

where the ac coupling coefficient, $\kappa = \kappa^*$, is given as

$$\kappa = \frac{\pi(\delta n_{eff})}{\lambda} \tag{4.13}$$

$\Delta\beta$, the general "dc" self-coupling coefficient for the uniform grating is given as

$$\Delta\beta = \delta + \sigma \tag{4.14}$$

where the dc coupling coefficient, σ, is given by

$$\sigma = \frac{2\pi\ \delta n_{eff}}{\lambda} \tag{4.15}$$

and the detuning, δ, is given as

$$\delta = 2\pi n_{eff}\left(\frac{1}{\lambda} - \frac{1}{\lambda_D}\right) \tag{4.16}$$

where $\lambda_D$is the design wavelength for Bragg scattering and and $\lambda = 2\ n_{eff}\Lambda$ is the Bragg wavelength.

From a system of equations, the initial reflectivity of the grating can be derived by assuming no reflection at the output of the grating i.e. A (z=L) =0 and B (z=0) =1. It is given as

$$R(L,\ \lambda) = \sinh^2(\sqrt{\kappa^2 - \Delta\beta^2}\mathrm{L})/\cosh^2\left(\sqrt{\kappa^2 - \Delta\beta^2}\mathrm{L}\right) - \frac{\Delta\beta^2}{\kappa^2} \tag{4.17}$$

Where R is the reflectivity, κ is the coupling coefficient given in the equation 4.13 and $\Delta\beta$ is obtained from the equation 4.14.

4.3 Choice of π-phase shifted fiber Bragg grating as the sensing element

A $\boldsymbol{\pi}$-PSFBG is an in-fiber optical filter that transmits a very narrow line width within a much broader reflection spectrum. Half a grating period is skipped during the fabrication in order to produce an extended gap in the center of a uniform grating. Consequently, two separate gratings are formed which act as an extended Fabry-Perot etalon and can select the transmitted wavelength. Backward propagating modes reflected from each of these gratings will be out of phase with each other by $\boldsymbol{\pi}$, hence named $\boldsymbol{\pi}$-PSFBG. Figure 4.1 illustrates the structure of a standard FBG and $\boldsymbol{\pi}$-PSFBG. Introducing a π phase shift in the middle of the FBG results in the formation of a narrow peak with a megahertz line width. Compared to the typical width of a FBG signal of tens of GHz, the signal of a π-PSFBG is much narrower. Therefore, sensors based on PS-FBG will offer much higher resolution compared to their FBG counterparts.

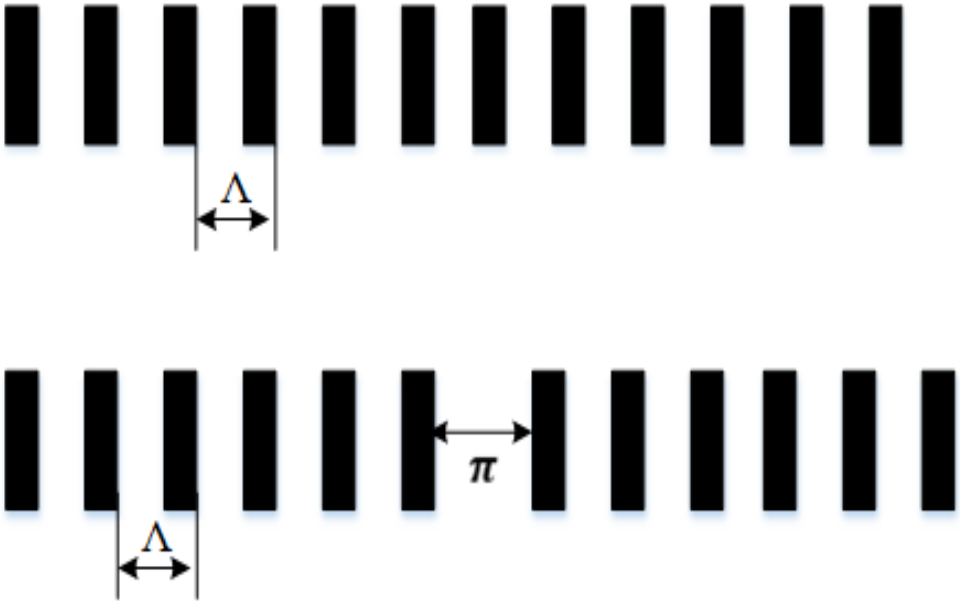

Fig. 4.1 Fringe structure of a typical FBG (top) v/s $\boldsymbol{\pi}$-PSFBG (bottom)

4.4 Simulation of the apodized π-PSFBG spectrum signal in MATLAB

A π-PSFBG spectrum is simulated in the steps shown in figure 4.2. Length of grating is 24 mm. Refractive index perturbations along the grating length, $\delta n_{eff}(z)$, are designed by equation 4.1. The peak to peak refractive index modulation is 3×10^{-4}. Two equal gratings sections are

designed using index perturbations with a gap of 0.276 μm (Λ/2) in the center. The refractive index of the gap between the two gratings is the same as of the core prior to grating inscription. The index is modulated with an apodization function after which the coupling coefficient as a function of grating length is simulated. Finally the coupling coefficients are substituted in the reflection equation, 4.17, to simulate the reflectivity v/s wavelength of the grating.

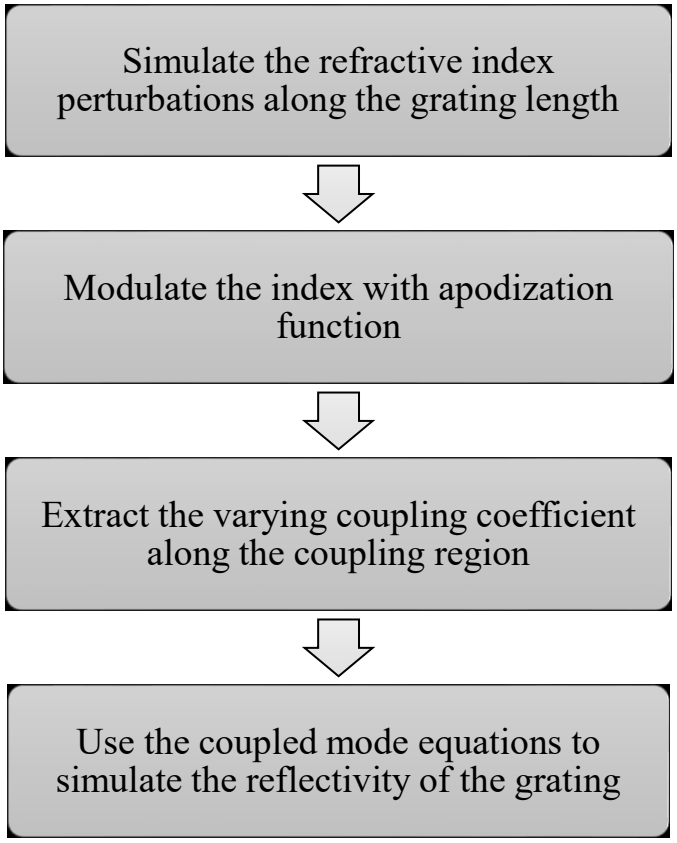

Fig. 4.2 The flowchart describing the step by step MATLAB simulation for output spectrum of π-PSFBG

The MATLAB simulation results of induced index change along the grating length, $\overline{\delta n}_{eff}(z)$, before and after apodization are shown in figure 4.3, a and b. The apodization profile that was proved to be better than the Gaussian profile in side lobe suppression is given by[41]

$$f(z) = 0.55 - 0.45cos(\frac{2\pi z}{L}) \tag{4.18}$$

In practice, this function is used to design an amplitude mask, which is placed between the laser and phase mask during grating inscription. Apodization profile provides a geometric shape to refractive index modulation, which is otherwise uniform in the unapodized grating. As seen from figure 4.3.b, the strength of refractive index is lower towards the end of the grating. This decreases the stop band and increases the transmission characteristics of the grating.

a)

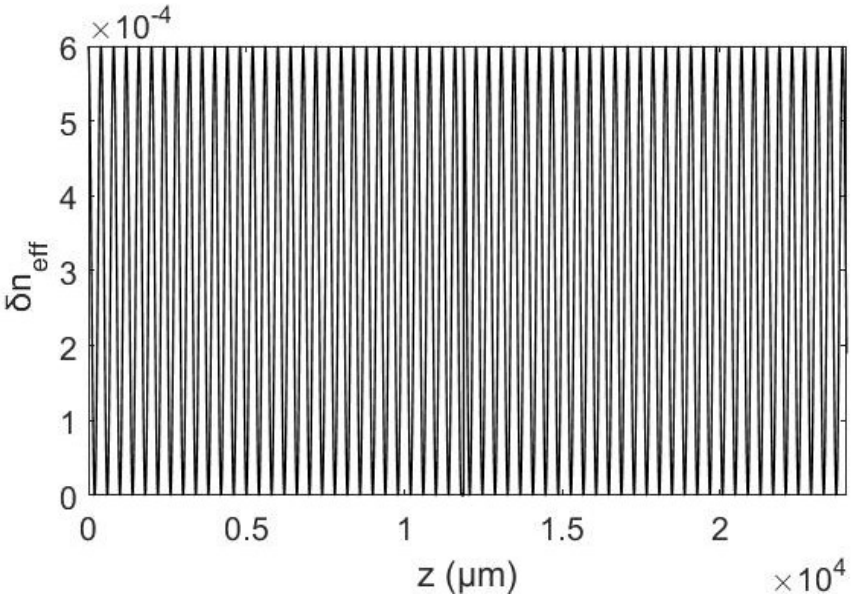

b)

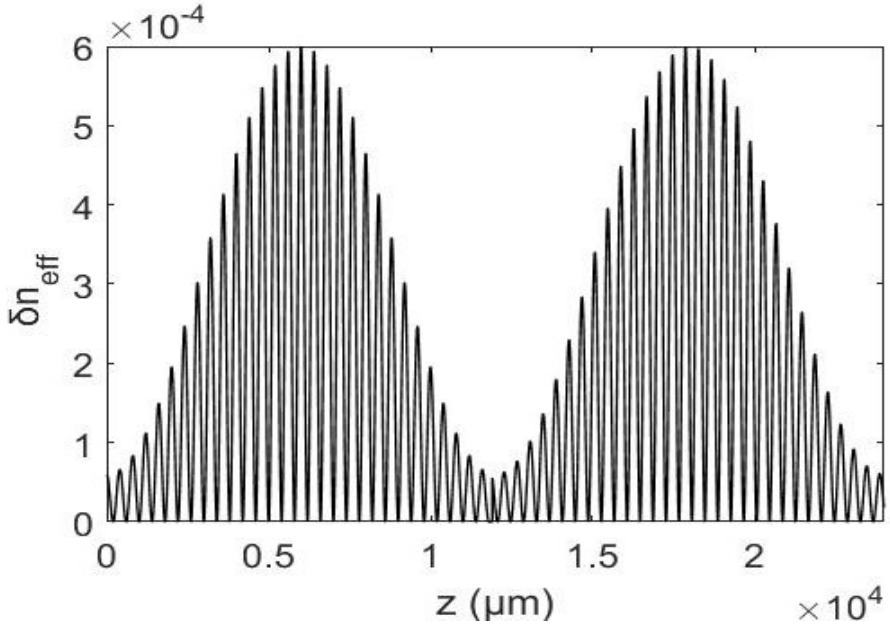

Fig. 4.3 Refractive index perturbation in **(a)** Unapodized $\boldsymbol{\pi}$-PSFBG. **(b)** Apodized $\boldsymbol{\pi}$-PSFBG.

Figure 4.4 shows the wavelength spectrum of π-PSFBG before (dashed line) and after (solid line) apodization for the index profile. The Bragg wavelength or the transmission notch is centered at 1543.220 nm and the full width at half maximum (FWHM) for this peak is approximately 20 pm. It can be observed that the side-lobes after apodization have significantly been suppressed. The stop band of apodized grating has decreased from approximately 2 nm to 1 nm because of the decrease in effective length of the grating caused by weak refractive index modulation at the beginning and the end of the grating (refer figure 4.3 b).

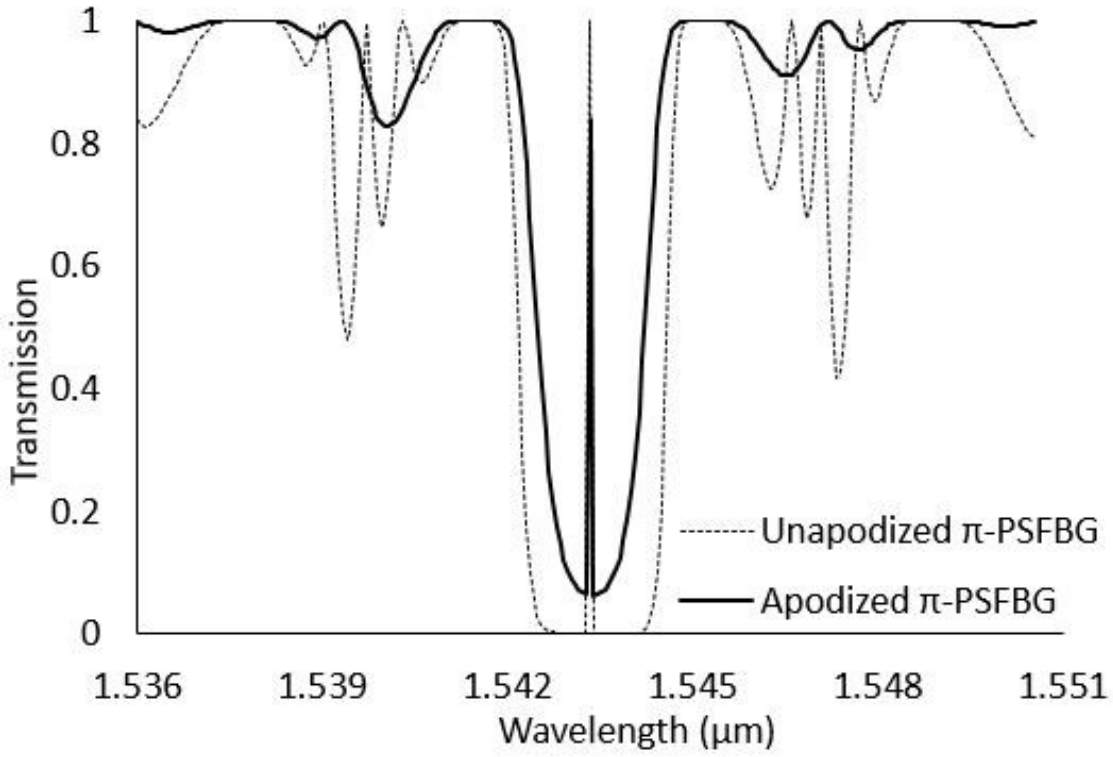

Fig. 4.4 Transmission spectrum of the $\boldsymbol{\pi}$-PSFBG before and after apodization

4.5 Strain sensitivity of the π-PSFBG

The change in grating period and effective refractive index govern the change in Bragg wavelength of the grating. Change in grating period is the result of the strain and change in the refractive index is induced from the temperature variations. Temperature also effects the grating period but around room temperature, the effect of temperature on refractive index is much larger than that on the grating period[8]. This impact is studied in MATLAB by considering the grating period variations

at RT over the range of 0.5 nm (from 499.7 nm to 500.2 nm) and tracing the Bragg wavelength shift of PSFBG with respect to it. Figure 4.5 shows the Bragg wavelength shift of 0.8 nm towards the higher wavelength observed due to the variations in the grating period.

The Bragg wavelength shift due to axial strain is given by the equation[47]

$$\Delta\lambda_b/\lambda_b = (1\text{-}P_e)\cdot\varepsilon \tag{4.19}$$

where P_e is the photo-elastic coefficient of the fiber and is equal to 0.22 and ε is the amount of strain induced on the fiber. According to the MATLAB simulations, the strain sensitivity of the FBG at 1542.9 nm is 1.2 pm/μ strain. The sensitivity of grating period with respect to strain is calculated as 0.7pm/ μ strain.

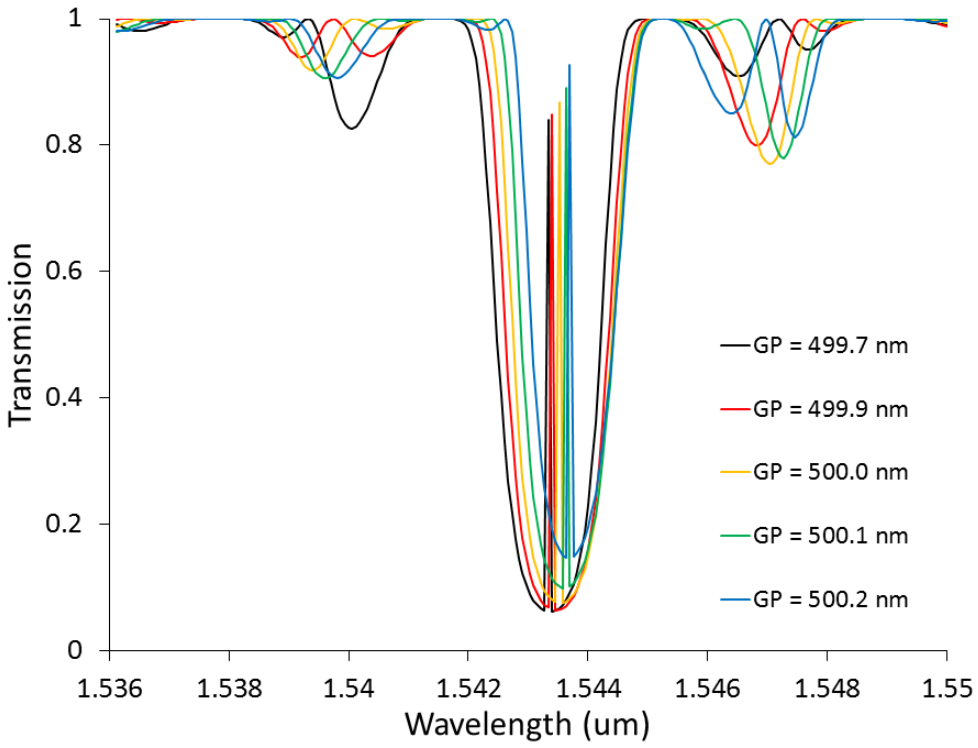

Fig. 4.5 Impact of changes in grating period on the Bragg wavelength of $\boldsymbol{\pi}$-PSFBG. Shift in the Bragg wavelength is 0.8 nm with respect to 0.5 nm of the change in grating period.

4.6 Temperature sensitivity of the π-PSFBG

Temperature has effect of altering the refractive index of both core and the cladding as well as the length of fiber. However, the length change associated with temperature contributes to only 10% of the overall change, therefore the change in refractive index is the dominating factor. Thus the effect on Bragg wavelength due to the changes in the temperature is governed by the equation[48]

$$\Delta\lambda/\lambda = (\alpha + \eta)\Delta T \tag{4.20}$$

where η is the measurement of the variation in refractive index due to temperature, also called the thermo optic coefficient of the fiber. It is represented as

$$\eta = 1/n \cdot \partial n/\partial T \tag{4.21}$$

and α is the thermal expansion coefficient which is the measurement of temperature induced fiber length expansion and is given as

$$\alpha = 1/\Lambda \cdot \partial\Lambda/\partial \mathrm{T} \tag{4.22}$$

The value of thermo optic coefficient and thermal expansion coefficient for a standard silica fiber are $8.6 \times 10^{-6}/°C$ and $0.55 \times 10^{-6}/°C$ respectively [39], [40]. Based on the MATLAB simulation results, the sensitivity of Bragg grating in wavelength range of 1550 nm is 14.18pm/ °C with respect to temperature.

Temperature compensation is a major concern in humidity sensor applications. To resolve this, a twin but uncoated FBG, is placed in the series with humidity sensing element inside the sensor. The coated grating detects humidity while the uncoated grating compensates temperature effect on humidity detecting peak.

4.7 Summary

In this chapter, the refractive index in the core of optical fiber was modulated with an apodization profile simulated using MATLAB. The spectrum of a **π**-PSFBG before and after apodization are simulated using the coupled mode theory. The sensitivity of the grating with respect to strain and temperature has been discussed and modeled.

5 π-PSFBG humidity sensor: Fabrication method

5.1 Aim

In chapter 3 and 4, eminent details regarding the humidity sensing element made out of polymer coated, apodized $\boldsymbol{\pi}$-PSFB have been modeled, simulated and discussed. This chapter focuses on the fabrication methodology of the modeled sensor. A combination of phase mask and amplitude mask are used to obtain the desirable apodization profile in $\boldsymbol{\pi}$-PSFBG, which is further coated with PI2525 polymer. In order to calibrate the fabricated sensor, a distributed feedback laser scanner setup is built with the help of QPS Photronics Inc. (A Quebec, CA- based company, specialized in fiber-optic sensors). The user interface used for monitoring the sensor response during calibration is designed in LabVIEW environment.

5.2 Making of the sensing element

Fiber optic sensors used in this work are two, 24mm long, π –PSFBGs on a SMF-28 fiber. Both the gratings are written 12mm apart thus making the entire sensor head of size 60 mm. The apodization profile from the model presented in chapter 4 is used during the fabrication. Sensors are made available from QPS Photonics Inc. Grating inscription and polymer coating processes are detailed in the following sections.

5.2.1 Fabrication of π-phase shifted fiber Bragg gratings

An excimer laser of maximum repetition rate 500 Hz, with nominal pulse energy of up to 7 mJ per pulse at 248 nm is used to write the gratings. Phase mask is used as a precision diffraction grating that divides the monochromatic incident beam into two beams. Amplitude mask is positioned between the laser and the phase mask as shown in figure 5.1. Function of the amplitude mask is to implement the apodization function derived from modeling in chapter 2. A gap of 0.279 μm (equivalent to Λ /2) is written in the middle of amplitude mask by splitting the apodization profile in center. Alignment marks are used to align amplitude mask with the phase mask. Self-interference between diffracted orders from phase mask produced the required pitch along fiber

length. This combination replaces the conventional fabrication technique of using $\boldsymbol{\pi}$-phase shifted phase masks and works equally well without the expense to make a new mask for every wavelength. The sensor head contains identical twin π –PSFBGs located 12 mm apart on a SMF-28 fiber. One of the gratings is coated with polymer (detailed in section 5.2.2) and the other is left uncoated. Both are placed in series inside the fiber. The polyimide coated grating is used for humidity measurement. Water molecules in the environment surrounding the sensor cause the polymer to swell and exert stress onto the grating. This stress can be recorded as the shift in transmission wavelength. Since polyimide coated grating is sensitive to both temperature and humidity, a compensation grating to isolate the humidity effect is required in the system. Second grating is used for temperature compensation.

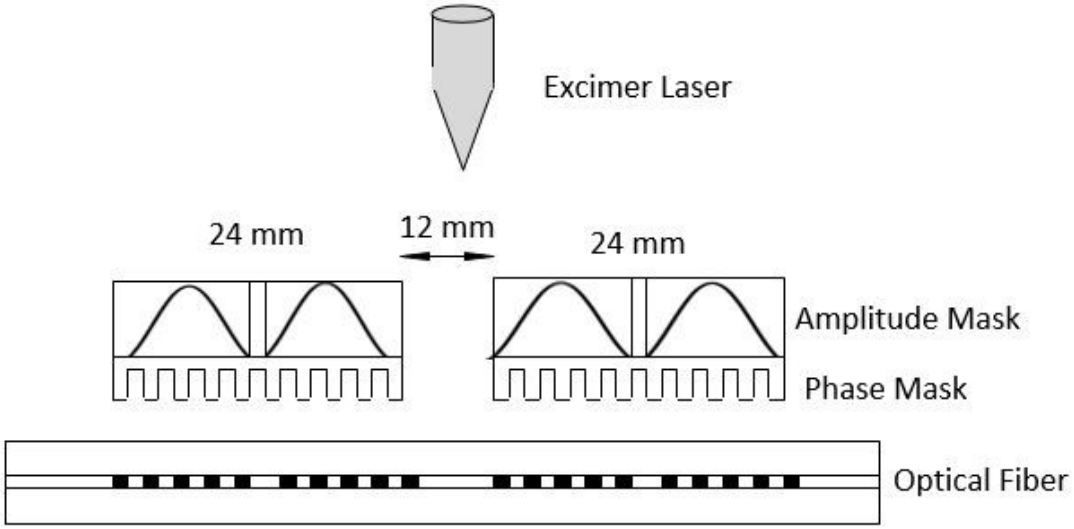

Fig. 5.1 Schematic showing the process of writing the gratings into the core of an optical fiber

The spectrum of resulting gratings has 0.1 nm wide stop band with 15 pm transmission window in its center. Figure 5.2 shows the spectrum of π – PSFBG humidity and temperature sensor at 27%RH and 22.8 °C. Here, transmission peak 1 with center wavelength around 1542 nm, functions as the humidity sensing element and peak 2 with center wavelength around 1542.135 nm is a temperature compensating element. Upon humidity ingress, polymer expands to exert strain on fiber hence altering the position of peak 1.

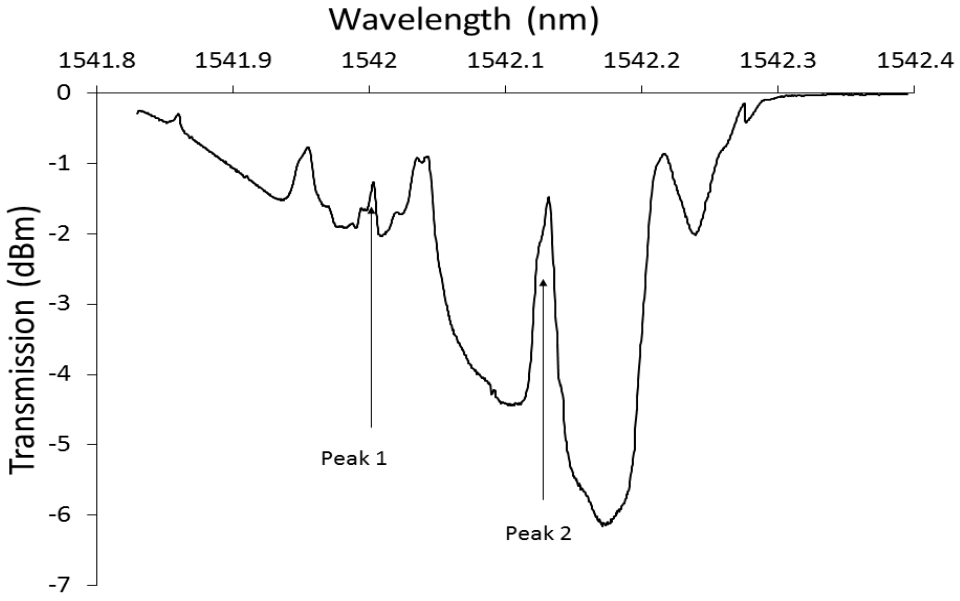

Fig. 5.2 Transmission spectrum of the proposed π-Phase shifted fiber Bragg grating humidity and temperature sensor produced using LabVIEW.

5.2.2 Polymer coating onto one of the gratings

The $\boldsymbol{\pi}$ − PSFBG is coated with polymer, polyimide (PI 2525, supplied by HD Microsystems) is a member of imidized polymer family. It is made from N-Methyl-2-Pyrrolidone, the structure of which has an imide linkage (carbonyl — amine — carbonyl), formed via a heterocyclic ring closure reaction. The cyclic rings impart thermal and mechanical strength to the polymer. Table 5.1 describes the properties of PI2525 as per the safety data sheet from the manufacturer.

Tensile strength (kg/mm²)	13.1
Dielectric constant (at 1 kHz, 50% RH)	3.3
Coefficient of thermal expansion (ppm)	40
Refractive index	1.70

Table 5.1 Properties of the material, PI2525, obtained from the manufacturer

The viscosity of polymer is (6 $\pm$ 1.0) $kg \cdot m^{-1} \cdot s^{-1}$ and thickness of 2 μm was obtained by controlling the withdrawal speed of fiber from the solution. Multiple dips were carried out to obtain the desired thickness of 20 $\pm 1 \mu m$. Finally, the coating is cured at 180°C for 2 hr. and then gradually cooled to the room temperature.

After the coating process, the signal spectrum of fiber grating coated with PI2525 undergoes a blue shift of 0.750 nm towards the lower wavelengths. Figure 5.3 shows the picture of the sensor head. One end containing the humidity-sensing element is connected to the interrogator and the other end towards the temperature-compensating element is left free.

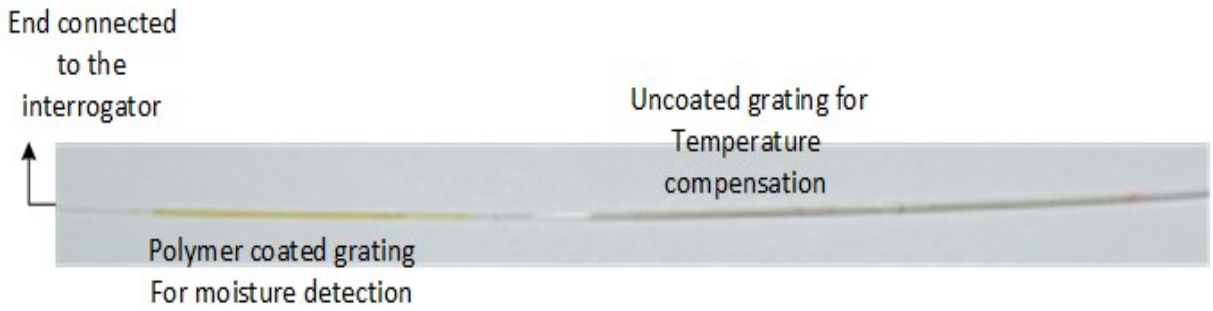

Fig. 5.3 Sensor head containing the humidity sensor and temperature-compensating element

5.3 Architecture of the sensor interrogator

To measure the humidity/temperature response of π-PSFBG sensor, an interrogator with resolution of +/-1 pm is required. We used a distributed feedback (DFB) laser scanner (provided by QPS Photonics Inc) for testing. The output is obtained at precise wavelength with narrow linewidth, low relative intensity and phase noise. DFB laser with center wavelength (1542.1 nm) is set in phase locked relationship of PS-FBG spectrum. Grating(s) to be interrogated is plugged in. The detection circuit is connected to a virtual instrument designed using LabVIEW, which calibrates the measurements each time data acquisition is performed. Architecture of the interrogator system is presented in figure 5.4.

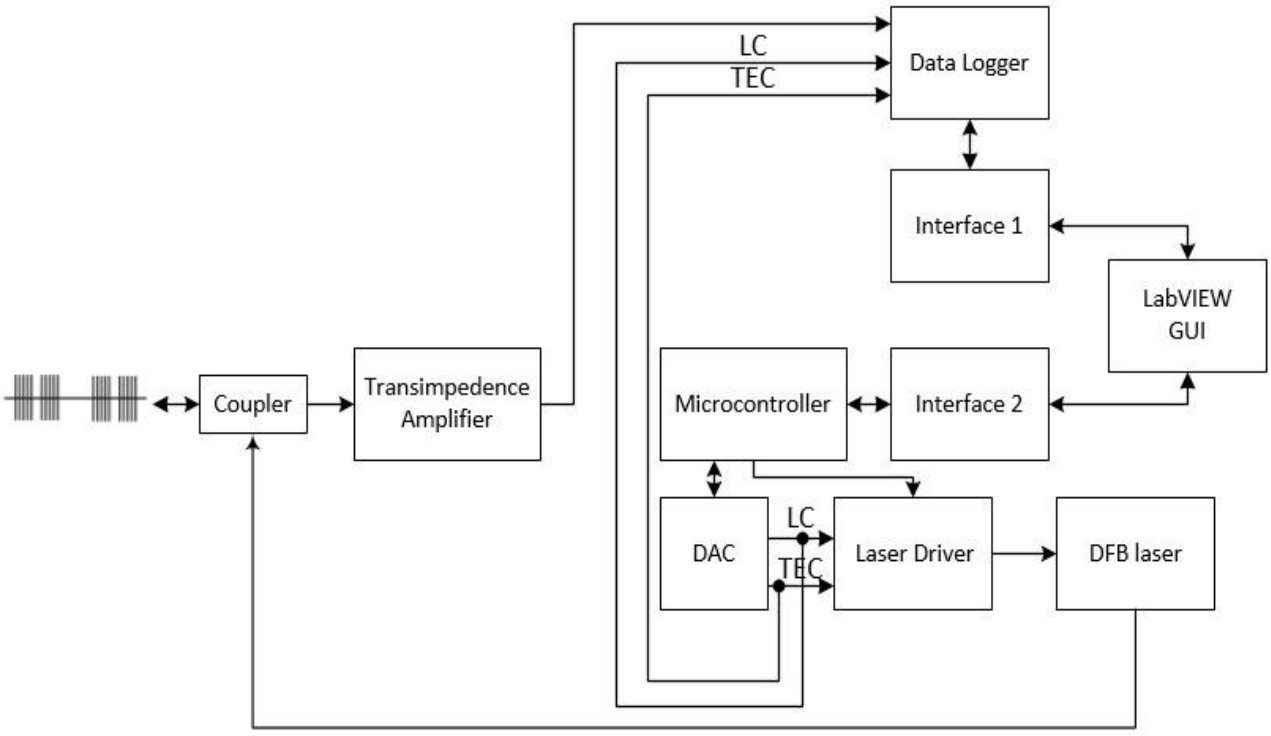

Fig. 5.4 Schematic of the distributed feedback laser scanner used as an interrogator for the sensor

5.3.1 DFB Laser

A distributed feedback laser (AlFOtec S/N 4147) centered at 1542.1 nm is used as a source to interrogate the sensor. It can be tuned in the range of about 3 nm. A microcontroller is used to modulate the laser via a laser driver using laser injection current control (LC) and thermo-electric cooler control (TEC). The resulting output is sent into the system through a coupler.

5.3.2 Coupler

A 1×2 coupler (DW12/15nm 1×2, OMC Industry Co Ltd.) is used in the system. It is built to function within two wavelength ranges, 1310±40 nm and 1550±40 nm. Optical signal from the laser passes through the optical coupler and splits into two outputs. One of the outputs reaches to the grating and the other is fed to a photodiode in a transimpedence amplifier.

5.3.3 Transimpedance amplifier

A receiver was made by connecting a photodiode to an amplifier. The optical signal introduced into the photodiode is converted into current, which is further converted into electrical voltages via a transimpedance amplifier.

5.3.4 Data logger

A 14 bit data logger (USB-6009, National Instruments) is used for analog to digital conversion. It has three channels, for LC, TEC and output from the TIA. The data-logger compiles the measurements of analog voltages from all the three channels.

5.3.5 Interface 1 and 2

LabVIEW user interface communicates with the interface 1 and 2 to send laser control commands to the interrogator and receive the output through the system. Interface 1 communicates with the data logger and Interface 2 is employed for communication with the microcontroller.

5.4 LabVIEW user interface

The DFB laser scanner is operated through an application designed using LabVIEW. Two USB ports (interface 1& 2 in the section 5.3.5) act as the communication links between the application and the interrogator. Settings are provided in the application to control the laser injection current sweep range and resolution. Similarly, variety of features is made available to control temperature sweep and resolution. These inputs affect the system through USB 2 (interface 2) that drives the laser driver. Any responses obtained from the system are coordinated back by the data logger to the application via USB 1 (interface 1). Figure 5.5 shows the main window of the application. Inputs triggering the sweep of LC and TEC are displayed towards the right half of the window. Left half of the screen contains response graph detected by the system. All the notches in the spectrum are auto detected and displayed in the list below the spectrum.

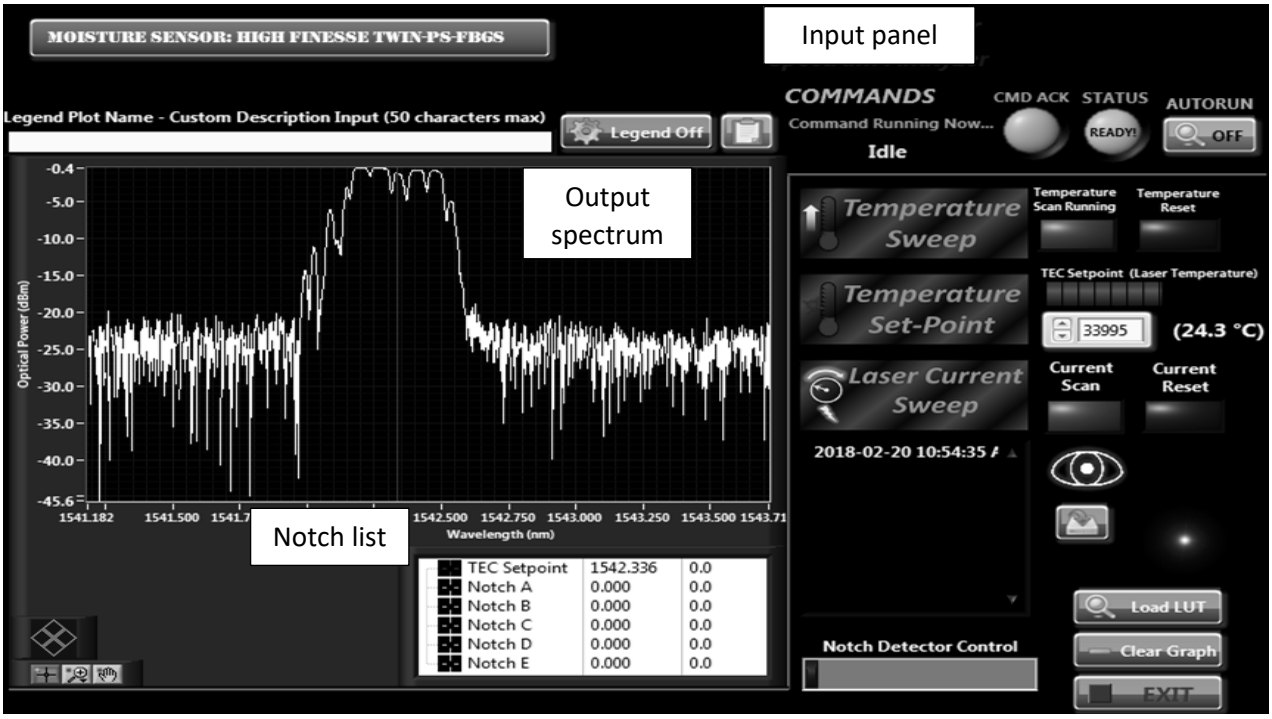

Fig. 5.5 LabVIEW application window for the sensor interrogation.

5.5 Summary

This chapter illustrated the fabrication of the π-PSFBG humidity and temperature sensor. Two 24mm long, π-PSFBGs are fabricated in a fiber- one is made to be humidity sensitive grating and the other functions to compensate the temperature cross sensitivity on the humidity sensitive grating. In order to calibrate the sensor, a distributed feedback laser scanner setup and LabVIEW user interface is explained in detail.

6 Experimental results

6.1 Aim

This chapter discusses the homemade experimental setups employed to measure the sensitivity of the sensor with respect to humidity as well as temperature. The sensor behavior with respect to the controlled changes in the environment around it is recorded through a series of experiments. The sensor is placed at constant temperature while the humidity around it is varied in the range of 20% RH to 50% RH. Response of sensor with respect to humidity is plotted and its sensitivity value is discussed. Response time of the sensor is recorded while monitoring the changes in sensor Bragg wavelength with respect to time when the humidity level is stepped up and down several times. For monitoring the sensor behavior with respect to temperature, experiments are conducted inside a temperature bath maintaining constant RH at 100% and changing temperature from 20-70 °C.

6.2 Experiment setup 1: Monitoring the humidity response of the sensor at constant temperatures

Series of experiments are conducted to determine sensor response with respect to changes in the humidity. A humidity chamber at room temperature is set up as shown in figure 6.1. A mixture of dry air and moisture is fed into the testing chamber. Changing the flow rate of dry air through the chamber, controls the level of RH inside it. For the reference, highly accurate humidity and temperature sensor with a remote probe was placed next to the π-PSFBG inside the chamber. The error for reference sensor was ±0.1%RH and ±0.04 °C for humidity and temperature respectively.

Series of commands are set into the interrogator through the PC containing LabVIEW application in it. This setup creates a repeatable (by ± 3%RH) and reliable environment for monitoring the sensor characteristics with humidity ranging 20% RH to 50 % RH.

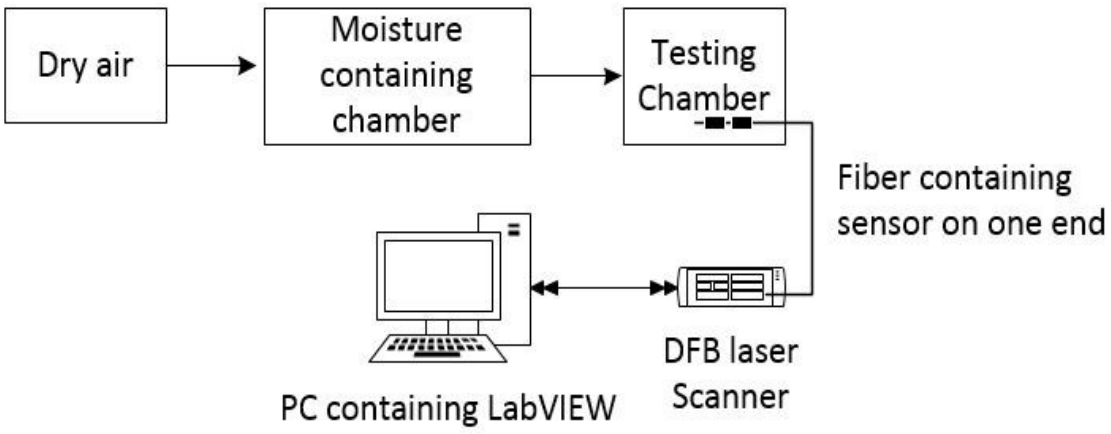

Fig. 6.1 Humidity chamber setup used for monitoring sensor characteristics with respect to changes in humidity at a constant temperature

6.3 Experiment setup 2: Monitoring the temperature response of the sensor at constant humidity

To illustrate temperature effect on PSFBGs, sensor is tested inside a temperature controlled water bath. It is secured inside a hollow tube of large diameter in order to protect it from other forces like water flow and stirring inside the water bath. The temperature of the water bath is varied in the range of 20 °C to 70 °C by the step change of 10 °C. A reference thermometer is used to make sure the temperature inside the hollow tube was the same as measured by the water bath. End of the sensor is connected to the interrogator and PC containing LabVIEW. Figure 6.2 shows the schematic of the experimental setup. Series of experiments are conducted, the results of which are discussed in the following section.

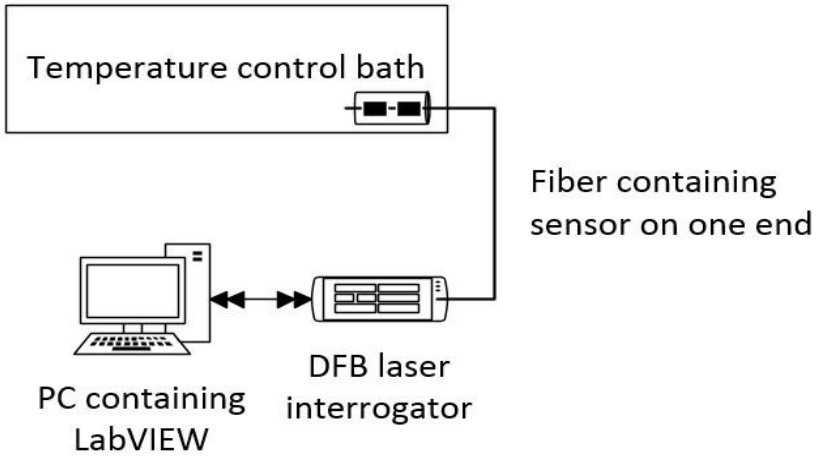

Fig. 6.2 Setup to monitor sensor characteristics with respect to the temperature changes.

6.4 Characteristics of the sensor with respect to humidity

Behavior of FBG transmission peak with respect to humidity is characterized in this section. Testing is done using the experimental set up explained section 6.2 and 6.3. Humidity inside the chamber is cycled up and down from 20% RH to 50% RH at 22.2 °C. The humidity sensitive peak shows the wavelength shift of (1.11 $\pm$ 0.02) pm/RH%. Figure 6.1 records the observations of this experiment. The change in transmission peak shows linearity as the humidity varies over this range. This is related to material expansion of polyimide coating due to increase in humidity inside the chamber. The up and down cycle shows some hysteresis in sensor behavior but the results show reversibility of the polyimide coating.

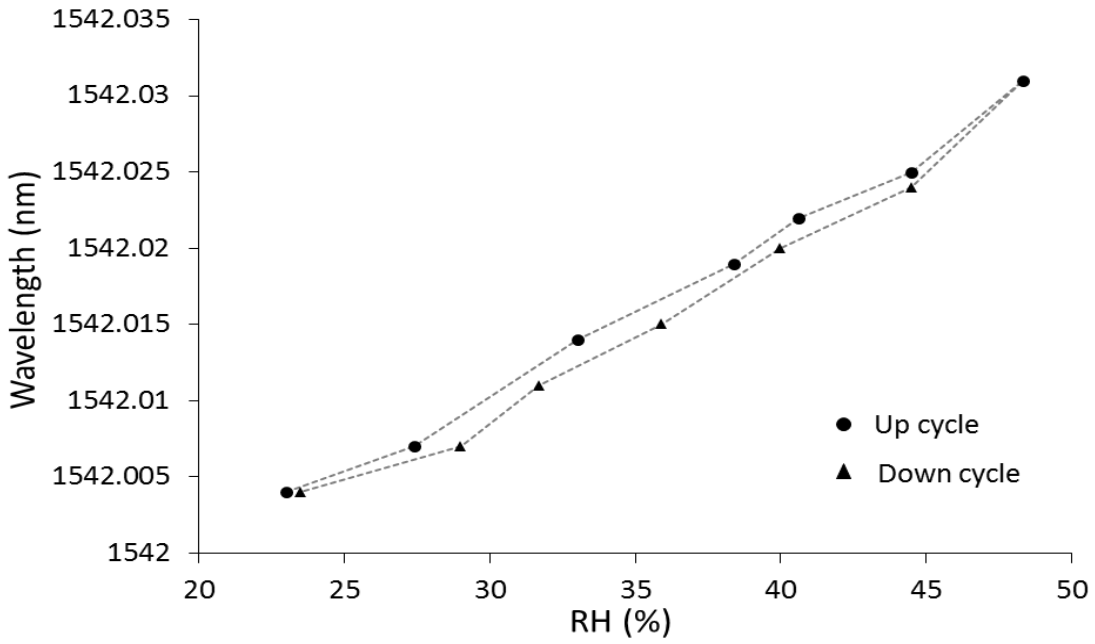

Fig. 6.3 π-PSFBG Transmission peak shift as a function of RH%. The up cycle refers to the increasing humidity from 20-50 % RH and the down cycle refers to the decreasing humidity from 50-20 % RH.

6.5 Response time of the sensor

The response time of the sensor is recorded while changing the humidity levels around it. Figure 6.2.a shows the shift in transmission peak with respect to time when humidity is changed in the range of 20% RH and 50% RH at 22.8 °C. It is observed that the sensor takes about 10 min to stabilize the reading. This result is comparable with the response time obtained using numerical analysis given in figure 3.11(b), where the mass uptake of polymer saturates after 9 minutes.

The time taken to stabilize the reading during the drying cycle is approximately 2.5 min. As figure 6.2.b shows, the wavelength at the end of drying cycle is the same as the wavelength at the beginning of wetting cycle. This shows that the polymer is completely reversible. It is also observed that the humidity desorption is faster than the absorption. This can be explained by the external factors like evaporation and the flow of air inside the humidity chamber. Since we have a

gas flow in the chamber, the evaporation from the surface and external layers of polymer induces an extra flux of humidity from the inner layers to the surface, which makes the drying cycle of 2.5 minutes approximately.

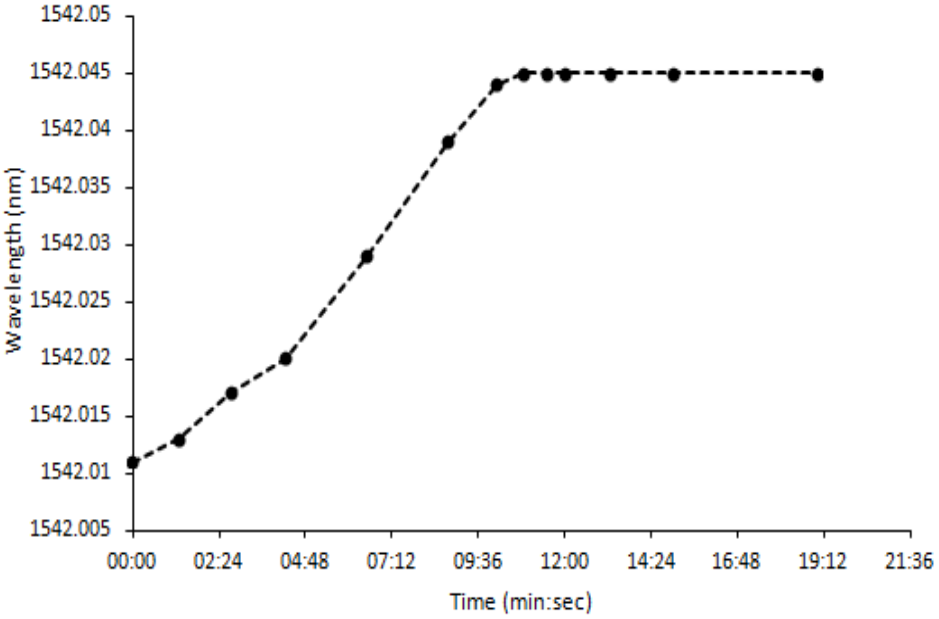

b)

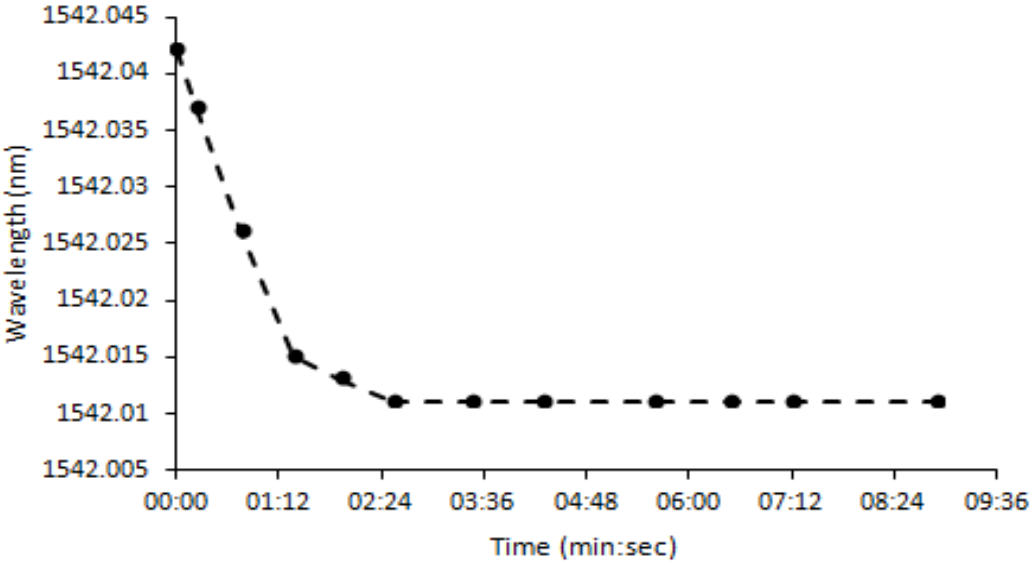

Fig. 6.4 Time response of sensor subjected to step humidity change **a)** from 21% to 48.3% RH **b)** from 48.3% to 21% RH, at 22.8 °C

6.6 Characteristics of the sensor with respect to temperature

To illustrate temperature effect on PSFBGs, sensor is placed inside a temperature controlled water bath. The sensor head is carefully placed inside the bath and temperature is varied by the step change of 10 °C. The findings show the wavelength shift of 10 ± 2 pm/°C at constant RH for both coated and uncoated FBG. A linear dependence of transmission wavelength with respect to temperature yields a total wavelength sweep of about 440 ± 12 pm over a range of 20°C to 70°C as it is presented in Figure 11. This result proves that at a constant RH%, the temperature response of both the gratings is quite similar and linear.

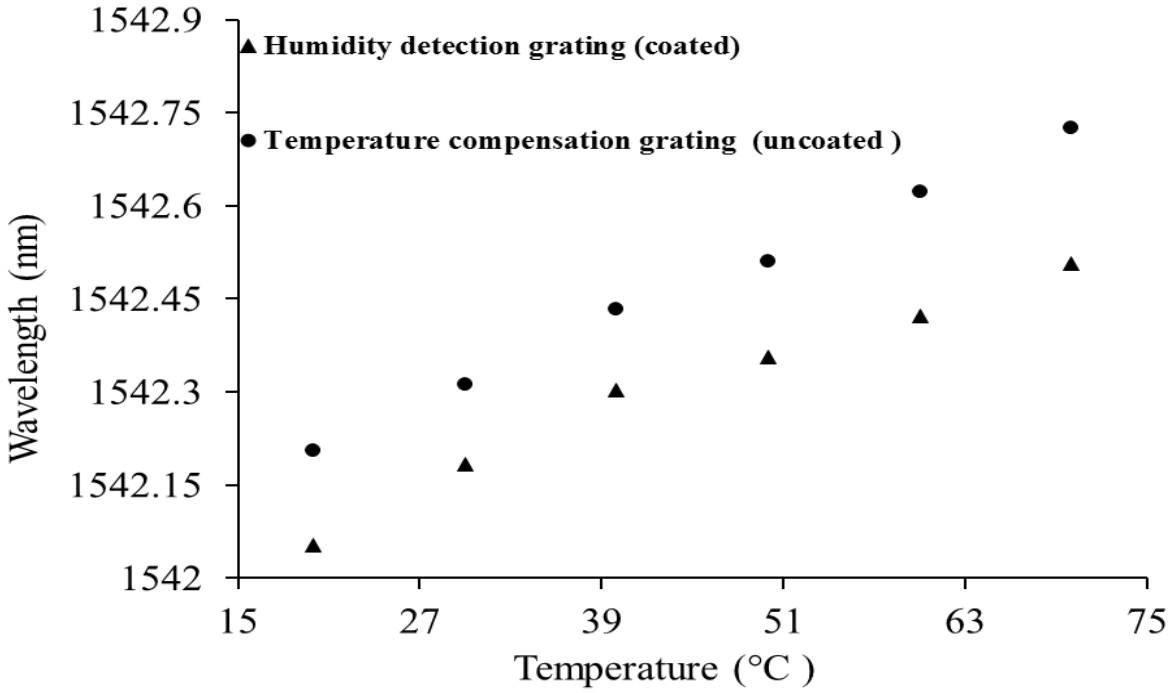

Fig. 6.5 Transmission response of the π -PSFBG sensor as a function of temperature (°C)

6.7 Summary

This chapter we have focused on the experimental results of sensor behavior with respect to the humidity and temperature around it. The design of experimental setups for measuring the

sensitivity of the sensor with respect to humidity as well as temperature are discussed. The sensor is placed at constant temperature while the humidity around it is varied in the range of 20% RH to 50% RH. Response of sensor with respect to humidity is (1.11 $\pm$ 0.02) pm/RH%. Response time of the sensor is about 10 min which is comparable with the response time obtained using numerical analysis using COMSOL (given in chapter 3, figure 3.11(b)). For monitoring the sensor behavior with respect to temperature, experiments are conducted inside a temperature bath maintaining constant RH at 100% and changing temperature from 20-70 °C. Results show that, as expected, both the gratings show similar response to the changes in temperature. The sensitivity of both the gratings is (10 $\pm$ 2) pm/°C at constant RH.

7 Conclusion and suggestions for future works

7.1 Conclusion

This thesis presents a design and development of an optoelectronic humidity and temperature sensor using polyimide coated, apodized π-PSFBG. This undertaking has brought us significantly better understanding of underlying mechanism of humidity absorption inside the polymer, which has been attributed to the mechanical deformation of the grating in the optical humidity sensor.

As discussed in chapter 2 and 4, the refractive index modulation in optical fiber Bragg gratings can be altered by applying strain and temperature to it. Decoding the shift of Bragg wavelength with respect to these alterations in refractive index is the criteria for humidity and temperature detecting optical sensors.

The structure and the performance of the sensor were first studied using COMSOL and MATLAB tools. A 24 mm optical sensor covered by layers of polyimide was modeled. Humidity transportation throughout the polyimide coating showed that

- The humidity absorption in polymer layer reaches a saturation point, which depends on the thickness of the polymer.
- Due to the volume expansion/contraction of the polymer a uniform and reversible force is exerted on the fiber.
- Water mass uptake by polymer is a function of time and is comparable with the experimental results.

To increase the sensibility of the sensor in terms of finer spectrum and lower side lobes, the core refractive index was modulated with an apodization profile simulated using MATLAB.

A sensor was fabricated based on the results of our modeling and simulations. Being a wavelength selective device, this sensor requires a wavelength discriminating system like a spectrum analyzer which would successfully decode the environmental changes in humidity and temperature. As per the requirements and application, a distributed feedback laser scanner was used to calibrate the sensor. Tests were conducted under various environmental conditions for its humidity, temperature

and response time characteristics. Response time of the sensor for increasing as well as decreasing humidity was measured.

- Measurements show the device has a 10 pm/°C sensitivity with respect to temperature between 20 to 70 °C.
- The sensor shows a very small hysteresis for up-down cycle of the humidity but is fully reversible.
- Observations show a good agreement between the experimental and theoretical results.
- This device can be very helpful in applications where other sensors fail due to possibility of operational hazards. One of such applications is to predict the ageing of transformers by detecting the moisture content of cellulose insulation inside it.

Further work is very important to envisage, enhance the stability and sensitivity, and explore the practice applications of this sensor.

7.2 Future direction

As seen in chapter 6, the sensitivity of grating with respect to humidity is (1.11 $\pm$ 0.02) pm/RH%. This value has a chance to be improved by increasing the thickness of the polymer coating or substituting the material of coating with a more hygroscopic polymer. However, there is a trade off because increasing the thickness of the coating also increases the sensor response time. Looking for other hygroscopic materials can be considered as the future tasks in order to further improve the quality of the sensor. Regarding the stability, the viability of fabricated sensors should be investigated in various environments such as concrete blocks. Studies of the degradation of the sensor over a long period of time and the cause of the degradation, and the ways to protect the sensor, are other suggestions for the future works in this area.

Decreasing the size of the sensor while maintaining its performance is one of the goals in industries to upgrade the device. Future work may include the investigation of smaller sizes in the range of 10 mm or 5 mm devices.

References

[1] Z. Chen and C. Lu, "Humidity Sensors: A Review of Materials and Mechanisms," *Sens. Lett.*, vol. 3, no. 4, p. 274–295(22), 2005.

[2] C. Zhang, X. Chen, D. J. Webb, and G.-D. Peng, "Water detection in jet fuel using a polymer optical fibre Bragg grating," in *Proc. SPIE 7503, 20th International Conference on Optical Fibre Sensors*, 2009, vol. 7503, p. 750380.

[3] H. Farahani, R. Wagiran, and M. N. Hamidon, *Humidity sensors principle, mechanism, and fabrication technologies: A comprehensive review*, vol. 14, no. 5. 2014.

[4] L. Gu, Q.-A. Huang, and M. Qin, "A novel capacitive-type humidity sensor using CMOS fabrication technology," *Sensors Actuators B Chem.*, vol. 99, no. 2–3, pp. 491–498, 2004.

[5] Z. M. Rittersma, "Recent achievements in miniaturised humidity sensors - a review of transduction techniques," vol. 96, pp. 196–210, 2002.

[6] K. O. Hill and G. Meltz, "Fiber Bragg grating technology fundamentals and overview," *J. Light. Technol.*, vol. 15, no. 8, pp. 1263–1276, 1997.

[7] G. Meltz; W. Morey; and W. Glenn, "Formation of Bragg gratings in optical fibers by a transverse holographic method." Opt. Lett. 14, pp. 823–825, 1989.

[8] B. Lee, "Review of the present status of optical fiber sensors," *Opt. Fiber Technol.*, vol. 9, no. 2, pp. 57–79, 2003.

[9] B.-O. Guan, H. Y. Tam, S. L. Ho, W. H. Chung, and X. Y. Dong, "Simultaneous strain and temperature measurement using a single fibre Bragg grating," *Electron. Lett.*, vol. 36, no. 12, pp. 1018–1019, 2000.

[10] H.-J. Sheng, M.-Y. Fu, T.-C. Chen, W.-F. Liu, and S.-S. Bor, "A Lateral Pressure Sensor Using a Fiber Bragg Grating," *IEEE Photonics Technol. Lett.*, vol. 16, no. 4, pp. 1146–1148, 2004.

[11] Y. Sadaoka, M. Matsuguchi, Y. Sakai, and Y. U. Murata, "Optical humidity sensing characteristics of composite thin films of hydrolysed nafion-dye with a terminal N-phenyl group," *J. Mater. Sci.*, vol. 27, no. 18, pp. 5095–5100, 1992.

[12] S. Otsuki, K. Adachi, and T. Taguchi, "A novel fiber-optic gas-sensing configuration using extremely curved optical fibers and an attempt for optical humidity detection," *Sensors Actuators B Chem.*, vol. 53, no. 1, pp. 91–96, 1998.

[13] Y. J. Rao, "Recent progress in applications of in-fibre Bragg grating sensors," *Opt. Lasers Eng.*, vol. 31, no. 4, pp. 297–324, 1999.

[14] H. Wang and Z. Zhou, "Advances of strain transfer analysis of optical fibre sensors," *Pacific Sci. Rev.*, vol. 16, no. 1, pp. 8–18, 2014.

[15] B. Torres, I. Payá-Zaforteza Ignacio, P. A. Calderón, and J. M. Adam, "Analysis of the strain transfer in a new FBG sensor for Structural Health Monitoring," *Eng. Struct.*, vol.

33, no. 2, pp. 539–548, 2011.

[16] L. Ren, J. Chen, H.-N. Li, G. Song, and X. Ji, “Design and application of a fiber Bragg grating strain sensor with enhanced sensitivity in the small-scale dam model,” *Smart Mater. Struct.*, vol. 18, no. 3, p. 035015, 2009.

[17] P. J. Thomas and J. O. Hellevang, “A fully distributed fibre optic sensor for relative humidity measurements,” *Sensors Actuators, B Chem.*, vol. 247, pp. 284–289, 2017.

[18] H.G.Limberger, P.Kronenberg, and Ph.Giaccari, “Influence of humidity and temperature on polyimide-coated fiber Bragg gratings,” *Bragg Gratings, Photosensit. Poling Glas. Waveguides*, no. July, p. BFB2, 2001.

[19] P. Kronenberg, P. K. Rastogi, P. Giaccari, and H. G. Limberger, “Relative humidity sensor with optical fiber Bragg gratings.,” *Opt. Lett.*, vol. 27, no. 16, pp. 1385–1387, 2002.

[20] K. M. Tan, C. M. Tay, S. C. Tjin, C. C. Chan, and H. Rahardjo, “High relative humidity measurements using gelatin coated long-period grating sensors,” *Sensors Actuators, B Chem.*, vol. 110, no. 2, pp. 335–341, 2005.

[21] L. Wang, Y. Liu, M. Zhang, D. Tu, X. Mao, and Y. Liao, “A relative humidity sensor using a hydrogel-coated long period grating,” *Meas. Sci. Technol.*, vol. 18, no. 10, pp. 3131–3134, 2007.

[22] X. F. Huang, D. R. Sheng, K. F. Cen, and H. Zhou, “Low-cost relative humidity sensor based on thermoplastic polyimide-coated fiber Bragg grating,” *Sensors Actuators, B Chem.*, vol. 127, no. 2, pp. 518–524, 2007.

[23] R. Aneesh and S. K. Khijwania, “Zinc oxide nanoparticle based optical fiber humidity sensor having linear response throughout a large dynamic range,” *Appl. Opt.*, vol. 50, no. 27, p. 5310, 2011.

[24] N. a David, P. M. Wild, and N. Djilali, “Parametric study of a polymer-coated fibre-optic humidity sensor,” *Meas. Sci. Technol.*, vol. 23, p. 035103, 2012.

[25] S. F. H. Correia, P. Antunes, E. Pecoraro, P. P. Lima, H. Varum, L. D. Carlos, R. A. S. Ferreira, and P. S. André, “Optical fiber relative humidity sensor based on a FBG with a di-ureasil coating,” *Sensors (Switzerland)*, vol. 12, no. 7, pp. 8847–8860, 2012.

[26] G. Rajan, Y. M. Noor, B. Liu, E. Ambikairaja, D. J. Webb, and G. D. Peng, “A fast response intrinsic humidity sensor based on an etched singlemode polymer fiber Bragg grating,” *Sensors Actuators, A Phys.*, vol. 203, pp. 107–111, 2013.

[27] A. J. Swanson, S. G. Raymond, S. Janssens, R. D. Breukers, M. D. H. Bhuiyan, J. W. Lovell-Smith, and M. R. Waterland, “Investigation of polyimide coated fibre Bragg gratings for relative humidity sensing,” *Meas. Sci. Technol.*, vol. 26, no. 12, p. 125101, 2015.

[28] W. Bai, M. Yang, J. Dai, H. Yu, G. Wang, and C. Qi, “Novel polyimide coated fiber Bragg grating sensing network for relative humidity measurements,” *Opt. Express*, vol. 24, no. 4, p. 3230, 2016.

[29] M. Hartings, K. O. Douglass, C. Neice, and Z. Ahmed, “Humidity responsive photonic sensor based on a carboxymethyl cellulose mechanical actuator,” *Sensors Actuators, B Chem.*, vol. 265, pp. 335–338, 2018.

[30] G. P. Agrawal and S. Radic, “Phase-Shifted Fiber Bragg Gratings and their Application for Wavelength Demultiplexing,” *IEEE Photonics Technol. Lett.*, vol. 6, no. 8, pp. 995–997, 1994.

[31] H. Wang, H. Guo, G. Xiao, N. Mrad, A. Kazemi, and D. Ban, “Phase-shifted fiber-Bragg-grating-based humidity sensor,” vol. 8720, no. May 2013, p. 872019, 2013.

[32] Q. Wu, Y. Okabe, K. Saito, and F. Yu, “Sensitivity Distribution Properties of a Phase-Shifted Fiber Bragg Grating Sensor to Ultrasonic Waves,” *Sensors*, vol. 14, no. 1, pp. 1094–1105, 2014.

[33] A. Ghatak and K. Thyagarajan, *Introduction to fiber optics*. Cambridge: Cambridge University Press, 1998.

[34] S. J. Mihailov, “Fiber bragg grating sensors for harsh environments,” *Sensors*, vol. 12, no. 2, pp. 1898–1918, 2012.

[35] K. O. Hill, B. Malo, F. Bilodeau, D. C. Johnson, and J. Albert, “Bragg gratings fabricated in monomode photosensitive optical fiber by UV exposure through a phase mask,” *Appl. Phys. Lett.*, vol. 62, no. 10, pp. 1035–1037, 1993.

[36] N. K. Sidhu, P. A. Sohi, S. Samadi, and M. Kahrizi, “Modeling of FBG Moisture sensor in COMSOL,” in *Photonics North (PN)*, 2018, p. 1.

[37] N. K. Sidhu, P. A. Sohi, and M. Kahrizi, “Polymer based optical humidity and temperature sensor,” *J. Mater. Sci. Mater. Electron.*, Jan. 2019.

[38] T. Erdogan, “Fiber grating spectra,” *J. Light. Technol.*, vol. 15, no. 8, pp. 1277–1294, 1997.

[39] M. Matsuhara and A. Watanabe, “Optical-waveguide filters: Synthesis,” vol. 65, no. July, 1975.

[40] I. Yulianti, A. S. M. Supa’at, S. M. Idrus, and A. M. Al-Hetar, “Simulation of apodization profiles performances for unchirped fiber Bragg gratings,” in *2010 International Conference on Photonics, ICP2010*, 2010.

[41] F. Chaoui, O. Aghzout, M. Chakkour, and M. El Yakhloufi, “Apodization Optimization of FBG Strain Sensor for Quasi-Distributed Sensing Measurement Applications,” *Act. Passiv. Electron. Components*, vol. 2016, 2016.

[42] M. McCall, “On the application of coupled mode theory for modeling fiber Bragg\ngratings,” *J. Light. Technol.*, vol. 18, no. 2, pp. 236–242, 2000.

[43] N. K. Sidhu, P. Kung, and M. Kahrizi, “Apodized Pi-PSFBG Moisture / Temperature Sensor,” in *Photonics North (PN)*, 2018, p. 1.

[44] A. W. Snyder, “Coupled-Mode Theory for Optical Fibers,” *J. Opt. Soc. Am.*, vol. 62, no. 11, p. 1267, 1972.

[45] D. Marcuse, “Coupled mode theory of round optical fibers,” *Bell Syst. Tech. J.*, vol. 52, no. 6, pp. 817–842, 1973.

[46] K. Okamoto, “Coupled Mode Theory,” *Fundamentals of Optical Waveguides*. pp. 159–207, 2006.

[47] M. Kreuzer, “Strain measurement with fiber bragg grating sensors,” *HBM, Darmstadt, S2338-1.0 e*, 2006.

[48] Z. Zhou and J. Ou, “Techniques of temperature compensation for FBG strain sensors used in long-term structural monitoring,” no. June 2005, pp. 167–172, 2005.